NASA

260-IN.-DIA MOTOR PROGRAM

FINAL REPORT
FOR MOTOR 44-SS-4

Contract NAS3-7970

5 June 1967

Prepared for

National Aeronautics and Space Administration
Lewis Research Center
Cleveland, Ohio

AEROJET
GENERAL TIRE
GENERAL

AEROJET-GENERAL CORPORATION

SACRAMENTO, CALIFORNIA

Requests for copies of this report should be referred to:

National Aeronautics and Space Administration
Office of Scientific and Technical Information
Attention: AFSS-A
Washington, D. C. 20546

AEROJET-GENERAL CORPORATION
AEROJET GENERAL TIRE GENERAL

SACRAMENTO • CALIFORNIA

SACRAMENTO PLANT

4 October 1967
SRO-67-5500C-L-126

National Aeronautics and Space Administration
Lewis Research Center
21000 Brookpark Road
Cleveland, Ohio 44135

Attention: Mr. H. E. Hinckley
Mail Stop 500-210

Subject: Transmittal of Report NASA CR 72287, 260-in.-dia
Motor Program, Final Report for Motor 44-SS-4

Reference: (a) Contract NAS3-7970

Gentlemen:

Enclosed is a copy of the subject report prepared on Contract NAS3-7970.

This is the final report submittal and completes the requirements of
Reference (a).

Sincerely,

AEROJET-GENERAL CORPORATION

A. J. Medved, Manager
Contract & Program Administration
Space Booster Division

AJM:bh

Encl: (1) NASA CR 72287 Report, dated 5 June 1967

cc: Distribution List, NASA/LeRC Ltr, Ref. 1444,
dated 2 October 1967

260-IN.-DIA MOTOR PROGRAM

FINAL REPORT
FOR MOTOR 44-SS-4

Contract NAS-7970

5 June 1967

Prepared for

National Aeronautics and Space Administration
Lewis Research Center
Cleveland, Ohio

TABLE OF CONTENTS

FIGURE LIST

FIGURE LIST (cont)

FIGURE LIST (cont)

I.   SUMMARY AND CONCLUSIONS

Motor 44-SS-4 was statically test fired successfully on 22 March 1967. Motor and nozzle performance were normal and valid data were recorded for every parameter over the entire test duration. Operation of all test systems and Special Test Equipment was normal.

Posttest condition of the nozzle liner and insulation was excellent. Despite the relatively short web-action time (12.10-sec), valuable data on the nozzle plastic and rubber insulation material loss rate and char depth was acquired which is directly applicable to the 260-SL-3 design and verifies positive margins-of-safety throughout the 260-SL-3 nozzle assembly.

The measured average material erosion and ablation at the nozzle throat was 0.040-in., resulting in a material loss rate of 0.0033-in./sec over the 12.1 sec web-action time. Erosion at the nose section (-2.0 area ratio) averaged 0.10-in. with selective higher losses (to 0.15-in.) noted adjacent to the grain valleys. Condition of the charred plastic surfaces was uniformly smooth with no gouges, chunking or other indication of abnormal performance. Erosion in the throat extension was negligible.

The shape of the actual and predicted chamber pressure-vs-time curves are very similar; however, the measured chamber pressure was higher than predicted, the actual maximum being 606 psia compared to a predicted pressure of 560 psia. This was due primarily to a propellant burning rate scale-up effect of approximately 3.6% over 3KS-500 burning rate data. The standard specific impulse obtained in the firing was 244.7-sec.

I, Summary and Conclusions (cont'd)

The 44-in.-dia motor was processed at the Aerojet-Dade Division, Homestead, Florida. Approximately 8000-lb of ANB-3254 propellant from the Lot 4 propellant materials qualification run were loaded in the insulated and lined Minuteman second-stage chamber. The propellant formulation and loading techniques used were the same as planned for motor 260-SL-3 and the acceptability of intended processing methods was demonstrated. After grain trimming and restriction, the loaded chamber was shipped to Solid Rocket Operations, Sacramento, for final assembly and test firing.

The nozzle assembly was fabricated by the Rohr Corporation, Space Products Division, Riverside, Calif. The nozzle design, materials, and manufacturing processes duplicated, as closely as possible, those used on the 260-SL-3 nozzle.

Although it is recognized that the relatively short duration of the 44-SS-4 motor limits the degree to which an ablative nozzle may be evaluated, sufficient performance data was obtained to substantiate the basic design, materials, and processing techniques used on the 260-SL-3 submerged nozzle. A performance prediction for the 260-in.-dia motor nozzle made on the basis of measured 44-SS-4 nozzle data, indicates that the 260-SL-3 nozzle will perform successfully.

The observed increase in effective propellant burning rate, when used in motors larger than 3KS-500 size, will be considered in making the final performance prediction for motor 260-SL-3.

I, Summary and Conclusions (cont'd)

In summary, all program objectives were accomplished, and data obtained from the 44-in. motor test gives no indication that abnormal performance should be expected from any 260-SL-3 motor component.

II.   OBJECTIVES

The principal objective of the 44-in. subscale motor program was to verify the design adequacy of the submerged nozzle for motor 260-SL-3 by evaluation of performance of a geometric subscale nozzle.

Secondary objectives were the determination of the processing characteristics and burning rate scale-up effect of ANB 3254 propellant.

III.   DESIGN DESCRIPTION

The subscale motor, designated 44-SS-4, was designed to be a direct scale-down of motor 260-SL-3 and to simulate as nearly as possible the internal gas flow conditions existing within the larger motor. The 44-SS-4 nozzle geometry and aft-grain design was scaled to the ratio of the throat diameters of the two motors, (15.5/89.1) or 0.174 to 1. Wherever feasible, the motor incorporated materials and fabrication or processing techniques specified for motor 260-SL-3, or proven in previous 44-in.-dia motor programs. The motor assembly (P/N 1128287) is shown in Figure 1. A brief description of the major components of the motor follows:

A.   CHAMBER

A second-stage Minuteman Wing I chamber (P/N 1-324410) was used for motor 44-SS-4. The chamber was fabricated of forged-and-machined Ladish D6aC steel having an ultimate tensile strength of 200,000 psi. The nominal

III, A, Chamber (cont'd)

cylindrical section I.D. was 44.160-in. and the chamber overall length was 120.158 in.

The forward head and the aft flange were machined from closed-die forgings, and the two cylindrical sections were machined from rolled-ring forgings. The cylindrical sections, forward head, and the aft flange were joined by girth welds. The thickness of the chamber was increased 50% in the weld areas.

The chamber incorporated integral skirt extensions, a forward igniter boss, and a nozzle attachment flange. The aft flange of the chamber mated with the nozzle by a shear-lip, axial-tension type bolted joint.

Chamber S/N 569788, originally acquired on Contract NAS3-6284, was furnished by the government for use on this program.

B.   CHAMBER INSULATION

The internal chamber insulation configuration* was the same as that of previous 44-SS motors. The insulation in the 44-SS motors was designed originally to simulate the fabrication and installation techniques used for 260-SL motor insulation. As a result, the chamber rubber thicknesses were much greater than would be required to provide thermal protection to the motor case for the relatively short 12 sec duration of motor 44-SS-4. The only change necessary was to increase the length of the aft boot extension 6.0-in. to facilitate casting the additional propellant grain length required.

---

*Volume IV: 260-SL Motor Internal Insulation System, Final Phase Report, Aerojet-General Report NASA CR-54930, 8 April 1966

III, Design Description (cont'd)

C.   PROPELLANT AND GRAIN

The grain configuration, shown in Figure 2, was similar to that used in the three previous 44-SS motors. The only change from the earlier configuration was in the aft portion of the grain. In the 44-SS-4 design, the grain was extended past the chamber aft flange and the aft face of the grain was chamfered. This change was made to provide the same relationship between grain and nozzle that will exist in motor 260-SL-3. The 44-SS-4 grain cross section, as in the previous 44-SS motors, was a scaled-down version of the 260-SL motor design.

The 44-SS-4 motor propellant was ANB-3254, the same propellant to be used in motor 260-SL-3. This propellant has a burning rate approximately 50% higher than that of the ANB-3105 propellant used in previous 260-SL and 44-SS motors. This burning rate increase was obtained by use of burning rate additives, and a finer blend oxidizer grind. Details of the development and qualification of ANB-3254 will be published in a 260-SL-3 Motor Program Final Phase Report. With this higher burning rate propellant, it was necessary to increase the nozzle throat diameter from the 13.1 in. of the previous 44-SS motors to 15.5 in. for motor 44-SS-4, to maintain chamber pressure within acceptable limits.

The same SD-850-2 liner system used in all 260-SL motors was used in motor 44-SS-4 to provide the bond between the propellant and the chamber insulation.

III, C, Propellant and Grain (cont'd)

To prevent propellant burning on the outside diameter of the trimmed aft-grain face, a nominal 0.388-in. thickness of IBT-106 was applied over this surface. IBT-106 is an Aerojet developed trowelable insulating material which is based on a PBAN and asbestos composition. The trimmed and restricted grain is shown in Drawing 1128285.

D. NOZZLE

The nozzle, as closely as possible, was a geometric subscale of the 260-SL-3 nozzle, except that the separate exit cone of the 260 nozzle was replaced by a lengthened throat extension. The entrance configuration of the fixed submerged design was a 1.5:1 ellipse starting at the 2.0:1 area ratio with a major semi-axis equal to 3/4 of the throat radius. The throat diameter was 15.5 in. The 17.5 degree conical exit section had an expansion ratio of 2.5:1. compared to 3.8:1 of 260-SL-3 motor. The nozzle design layout is shown in Figure 3.

The steel structure was a two-piece design, assembled with a threaded joint, using a shell of heat-treated AISI 4130 steel with a 160,000 psi minimum yield strength, and an entrance ring of normalized AISI 4130 steel of 70,000 to 100,000 psi yield strength. An AISI 1020 steel retainer ring was bolted to the aft flange as a redundant restraint on the throat extension insert.

The nozzle ablative insert design incorporated the same materials and processes that are specified for the 260-SL-3 nozzle inserts. The materials were Fiberite MX-4926 phenolic impregnated carbon cloth for the ablative surfaces and U.S. Polymeric FM-5131 phenolic impregnated silica cloth for the

III, D, Nozzle (cont'd)

reinforcing insulation and the aft-end of the submerged insert ablative

surface. The laminate orientation of the throat extension insert (25 to 35

degrees relative to the nozzle centerline), the submerged insert (75 to 90

degrees), and the nose insert (a combination of 82 to 97 degrees and parallel-

to-centerline) was the same as the 260-SL-3 design. The 44-SS-4 throat insert

combined the functions of the entrance and throat inserts of the 260-SL-3,

using a compromise laminate orientation of 52 to 67 degrees.

The nozzle shell and entrance ring insulation components were

layups of Gen-Gard V-44 silica-and asbestos-loaded butadiene acrylonitrile

rubber vulcanized to the steel. The rubber thickness at the step-joint

(40-in.-dia) was designed to match the existing 44-SS chamber insulation

thickness in this area. Rubber thickness loss data in the area adjacent to

and downstream of nozzle submergence is not well defined, particularly in

motor configurations where nozzle submergence depth is relatively low, such

as in motor 44-SS-4. Test firings of motors with submerged nozzles, such as

the second-stage Minuteman and the Thiokol 65- and 120-in.-dia motors, show

that at some point behind and downstream of the nozzle entrance the gas flow

velocity becomes stagnant, and rubber erosion is similar to erosion occurring

at the forward head. However, the exact area where the gas flow stagnates

is almost totally dependent on the specific configuration. For motor 44-SS-4,

it was assumed that full gas velocity would be attained at an area ratio of

approximately 2.5, which corresponds to a gas velocity Mach number of 0.24.

III, D, Nozzle (cont'd)

The observed thickness loss rate of V-44 rubber at this Mach number is 0.058 in./sec. Assuming an exposure time of 14 sec and a 1.25 factor of safety, the design thickness is calculated as follows:

$$t_{NS} @ = 2.5 = S.F. \left[(\theta) (TLR) \right] = 1.25 (14)(.058)$$

$$t_{NS} @ = 2.5 = 1.0 \text{ in.}$$

The nozzle shell insulation contour was then established by a line from the step-joint through the design thickness at the 2.5 area ratio (approximately 24.5-in.-dia), as shown in Figure 4.

IBT-100, an Aerojet developed trowelable insulation, was applied in the cavity between the entrance and the nozzle shell to approximate the 260-SL-3 contour.

E.   IGNITION SYSTEM

Ignition of the previous three 44-SS motors was accomplished by aft-end propellant-type igniters. For motor 44-SS-4, conventional head-end ignition was desired to facilitate the use of an "existing" system and reduce tooling and test costs.

The ignition system is shown in Figure 5. Available second-stage Minuteman motor igniters did not produce sufficient energy for reliable ignition of this motor. It was decided to adapt an existing 260-SL ignition motor booster (P/N 600270-19, S/N 260-IMB-07) for this application. The 260-SL ignition motor booster is a slightly modified Polaris B-3 first-stage motor igniter, as described in Aerojet-General Report NAS CR-54454, dated 20 August 1965. The

III, E, Ignition System (cont'd)

main charge contained a 1400 gram Alclo-Iron* mono-perforated, cylindrical

grain; the primary charge contained a solid 1.0-in.-dia x 1.0-in.-long,

78 gram Alclo-Iron grain. The energy delivery of this igniter in relation

to the 44-SS-4 motor configuration was as follows:

1400 grams x 2.17 x 10^3 cal/gram = 3040 x 10^6 calories

The initial propellant burning surface area of 44-SS-4 is 13,700 in^2.

13,700 in x 6.45 cm^2/in^2 = 88.4 x 10^6 cm^2

The total available energy is:

$$E' = \frac{3040}{88.4} = 34.4 \text{ cal/cm}^2$$

The effective burning duration of the 260-SL ignition motor booster

grain is 0.10 sec; therefore, the energy delivery rate or induced heat-flux is:

$$\bar{q} = \frac{34.4}{0.10} = 344 \text{ cal/cm}^2\text{-sec}$$

As shown in Figure 6, these values are well within the desirable energy range

required for reliable motor ignition.

The 1400 gram main charge (P/N 600269-9) and the 78 gram primary

charge (P/N P-1971274) were assembled to a special adapter (P/N 1128281) to

facilitate installation of the 5.0-in.-dia igniter into the 3.25-in.-dia

igniter boss through the aft-end of the motor. A threaded retention device

(P/N 1128282) was designed to secure the igniter in position during motor

operation.

Initiation of the igniter was accomplished by 2.0 grams of Alclo

pyrotechnic powder and a Hi-Shear PE 451-003 power cartridge. The exploding

---

*Alclo-Iron: 32.9% aluminum, 58% ammonium perchlorate, 0.5% Sterotex binder, 8.6% iron filler (r_b = 0.033P_c $^{.719}$ P_c = 1000 psia)

III, E, Ignition System (cont'd)

hardware (EBW) power cartridge was actuated by 2000 vdc, discharged from a
0.5 microfarad capacitor.

IV.   FABRICATION AND PROCESSING

A.   CHAMBER INSULATION

The chamber, S/N 569788, was insulated in February 1964, by the
Goodyear Tire and Rubber Co., in Akron, Ohio. This insulated chamber was
shipped to the Aerojet-Dade Division and was stored in the main Aerojet
warehouse in Homestead, Florida.

Prior to abrading and lining, the interior of the insulated
chamber was visually inspected for evidence of possible damage or material
degradation during the 2.5 year storage period. Only three minor defects
in the aft boot-to-insulation bond were detected; these were easily repaired
by filling with Epon 948.2 adhesive. Shore A hardness measurements taken on
the insulation and boot rubber indicated no material deterioration had occurred
during the storage period. The Vistanex material used as a temporary cement
to hold the propellant boots in place exhibited considerable deterioration
and was removed. The boots were held in place during processing with pressure
sensitive tape.

B.   MOTOR PROCESSING AT AEROJET-DADE DIVISION

1.   Preparation for Casting

The chamber internal insulation surface was prepared for the
lining operation by grit blasting with No. 50 aluminum oxide grit to abrade
the surface. The surface was then cleaned with solvent dampened rags and
dried at +165°F for 3 days.

IV, B, Motor Processing at Aerojet-Dade Division (cont'd)

A nominal 0.035 in. thickness of SD-850-2 liner was applied to the internal insulation surface to be in contact with propellant. The material was applied using special trowels (T-450170, T-450174) to obtain the desired thickness. The trowel screed marks were smoothed over using stiff bristle brushes. Scattered voids and liner-thin areas were detected after completion of the lining operation. These areas were repaired by local application of additional SD-850-2. The liner was cured at 80°F for 48 hr followed by 48 hr at 135°F. The chamber was rotated 90 degrees every 15 min. during the first 12 hr of the cure period. A total of 38.8 lb of SD-850-2 was required to line the chamber.

At the completion of liner cure, the chamber was placed in the handling harness, erected to the vertical position, and the core and casting adapter installed. The basic 44-SS core, T-450046, was modified to enable casting of the grain to the longer length required to provide the desired scaling geometry and motor performance. This was accomplished by the addition of a 6-in. core section removed from the aft-end of a duplicate core which was to be scrapped.

The conditioning shroud was placed around the chamber and heated air was applied until the core thermocouples indicated +135°F. This temperature was maintained until the chamber was positioned for casting.

2. Propellant Casting

Propellant loading was conducted on 16 December 1966, using ANB-3254 propellant from the Lot-4 propellant qualification run. Approximately

IV, B, Motor Processing at Aerojet-Dade Division (cont'd)

8300 lb of propellant from batches B-468 and B-469 processed in the vertical batch mixers, were cast in the motor.

The casting technique was essentially the same as that used on 260-SL motor loading operation. A three-way manifold and valve assembly connects three bayonets to the propellant pot. The pressurized propellant pot was suspended above the motor by the stiffleg derrick which varied the pot height to maintain the specified bayonet submersion depth (below the propellant level) of 6 to 12 in. New casting bayonets were used for the second propellant batch.

The ANB-3254 propellant exhibited excellent processing characteristics. Propellant flow and adhesion to the sidewall liner were normal. The bond strength of ANB-3254 propellant to SD-850-2 liner was tested in tension and shear for each of the two propellant batches. All samples failed at random within the propellant, indicating a bond strength in excess of the cohesive strength of the propellant.

The casting operation was normal in all respects and was completed in less than 5 hr. Ballistic and physical property acceptance data from the two batches used for this motor are summarized in Figure 7.

   3.   Post Cast Operations

      a.   Cure

         Immediately following propellant loading, the motor began its cure cycle. Dry, heated air at +135°F was circulated within the conditioning shroud for 17 days. The propellant initial modulus (E_o) had

IV, B, Motor Processing at Aerojet-Dade Division (cont'd)

reached an average value of 515 psi at this time, very close to the target of 500 psi. Physical property data-vs-cure time is shown in Figure 8. Figure 9 summarizes burning rate and constant strain data obtained from the cured propellant.

b.   Cool Down and Core Removal

Following cure, cooling air (+65°F) was circulated around the motor until the core thermocouples indicated 100°F or lower.

On 6 January 1967, the core was removed from the cured and cooled grain. No difficulty was experienced and a stripping force of approximately 1500 lbf was recorded, well within the established limits.

c.   Grain Trim and Restriction

The aft-end of the propellant grain was trimmed to the final configuration shown in Figure 2, and dimensionally accepted using trim template T-1005411. The aft-grain profile represents a subscale configuration of the 260-SL-3 grain and is shown after trimming in Figure 10. The weight of the trimmed propellant grain was 7930 lb.

The O.D. of the aft-grain extension was restricted with a 0.388-in. nominal thickness of IBT-106, a trowelable PBAN based insulation material. The optimum processing and application techniques for this material were developed during the course of the program.

Thickness control of the applied restriction was maintained by bonding previously cast and cured strips of IBT-106 (0.50-in.-wide by 0.388-in.-thick) to the trimmed grain surface with uncured IBT-106. After

IV, B, Motor Processing at Aerojet-Dade Division (cont'd)

the bonding surface had cured, a brush coat of IBT-106 was applied to the entire surface to be restricted, followed by the final application using an elongated nozzle on the Semco pressure gun. The final surface contour and thickness were obtained by smoothing with small screeds between the guide strips. Curing at 135°F for 48 hr completed this procedure. Figures 11 through 13 show various phases of the restriction operation.

The quality of the completed restricted grain assembly met all requirements of Drawing 1128285. There were no inspection reports issued nor discrepancies detected during the casting or postcasting motor processing.

d. Motor Shipment

The loaded 44-SS-4 motor was transported from Aerojet-Dade Division to Solid Rocket Operations (SRO), Sacramento, in a Minuteman second-stage motor transporter (Utility Van). The motor departed on 31 January 1967 and arrived at Sacramento on 6 February 1967. The van interior was maintained at 80 ± 5°F during the trip.

C. NOZZLE

1. Structural Components

The nozzle steel components were fabricated in accordance with Aerojet Drawings 1127943, Nozzle Entrance Ring; 1127942, Nozzle Shell; and 1128114, Retainer Ring.

The nozzle shell was fabricated by TIG welding three ring-forgings and two roll-and-weld cones, all of vacuum-degassed AISI 4130 steel,

IV, C, Nozzle (cont'd)

using Linde 71B filler wire; heat treating to a minimum tensile yield strength of 160,000 psi (actual - 190,000 psi avg.); and machining to final dimensions. An error in the fit-up of the components for the circumferential welds caused the heat-treated weldment to be too short to meet the dimensional requirements of AGC Drawing 1127942. As reported in SDAR 34281, and as shown in Figure 14, a deviation was allowed from the drawing requirements such that the forward flange was translated aft 0.300 in. relative to the forward cone. Structural analysis of this change indicated that a negligible increase in the chamber attach bolt load would result. To preserve the submerged nozzle-to-propellant grain contour relationship, the remainder of the nozzle shell was also translated forward 0.300 in. relative to the forward cone, resulting in a reduction in the nozzle shell insulation design thickness by 0.21-in. and shortening of the throat extension and overall length by 0.150-in. The margins of safety for the shell were unaffected by this deviation, but the insulation minimum factor of safety was reduced from 2.0 to 1.4.

The nozzle entrance ring was machined from a forging of vacuum degassed AISI 4130 steel normalized to an average tensile yield strength of 92,400 psi. No significant discrepancies were encountered.

The retainer ring was torch cut from 1020 steel, stress relieved, machined and drilled to drawing requirements.

2. Rubber Insulation

The rubber insulation on the nozzle shell and entrance ring was laid-up on the steel to the required thickness using 0.125-in.-thick

IV, C, Nozzle (cont'd)

Gen-Gard V-44 silica and asbestos-filled butadiene acrylonitrile rubber sheet stock. As shown in Figure 15, a dam was installed at the step-joint to facilitate overbuild. The steel surface was prepared for bonding by application of Thixon P-4 primer and Thixon XO-1209 adhesive. The layups were vacuum bagged and autoclave cured at 310°F.

Machining of the entrance insulation and the mating surfaces of the shell insulation concluded fabrication operations on the insulation, as shown in Figure 16. No exceptions to the requirements of Aerojet Drawing 1127945, Nozzle Entrance Assembly, were reported. A small void located at the step joint of the shell insulation was filled using the repair method of Specification AGC-36420, Paragraph 3.4.4.2.3. The 0.78 dimension of Aerojet Drawing 1127944, Nozzle Shell Assembly, on the leading edge of the step-joint was rounded off to an undersize condition as reported on SDAR 34319.

3. Plastic Components

The ablative plastic inserts are composites of phenolic impregnated carbon cloth (Fiberite MX-4926) and phenolic-impregnated silica cloth (U.S. Polymeric FM-5131), where the one material is preformed to essentially the final cured density prior to application of the second material. The typical billet is fabricated by tape wrapping bias-cut carbon cloth on a mandrel to a target density; preforming at 1000 psia and 175°F in a hydroclave; machining the preformed billet; overwrapping parallel to the surface with warp-cut silica cloth; and final curing at 1000 psia and 300°F in a hydroclave. For the 44-SS-4 nozzle design, some unique configuration requirements necessitated different techniques and approaches.

IV, C, Nozzle (cont'd)

The throat extension insert (P/N 1127944-1) was fabricated in the conventional manner, similar to the corresponding 260-SL-3 insert, with the carbon cloth wrapped at 35 degrees relative to the nozzle centerline on a 17.5 degree conical mandrel, expecting a laminate reorientation to 25 degrees. No discrepancies were reported for this insert, which is shown being prepared for final machining of the overwrap in Figure 17.

The carbon cloth for the throat insert (P/N 1127945-1) was wrapped at a starting angle of 67 degrees on a 2 degree conical mandrel. The predicted laminate orientation after debulk was 52 degrees. The silica cloth overwrap was applied in the form of full-width bias-cut tape using a special double-cone roller to avoid traversing across the intersection of the conical surfaces required for the carbon-to-silica interface (Figure 3). The only reported discrepancy for the throat insert was that the 150°F devolatilization hold period in the cure cycle was 10 min shorter than planned (SDAR 34269).

Because of the unusual composite laminate orientation requirements of the nose insert (P/N 1127945-3) (Figure 3), two carbon cloth billets were wrapped and preformed separately. The preforms were match-machined, assembled with a phenolic resin interface, and again machined for application of the silica cloth overwrap. The overwrap was actually a hand layup of broad-goods (as was the counterpart insert for the 260-SL-3 nozzle) because of the problems associated with tape wrapping on a variable-angle surface and because the silica component is essentially an inlay at the outer diameter.

IV, C, Nozzle (cont'd)

The perpendicular-to-centerline carbon cloth billet for the nose insert was wrapped at a starting angle of 95 degrees relative to the centerline on a 30 degree conical mandrel. The laminate reorientation during preform debulk was expected to result in a minimum angle of 82 degrees.

The parallel-to-centerline carbon cloth billet was wrapped with warp-cut tape on a cylindrical mandrel and overwrapped with a nylon tension wrap prior to the preform cycle to avoid significant wrinkling during debulk. The desired effect of the tension wrap was achieved in that the compression of the outer plies was uniformly distributed, resulting in a barely preceptible wavy appearance on the outside diameter.

Three discrepancies reported for the nose insert resulted from machining errors on the preformed billets. SDAR 34310 reported that the required three specimens for microtensile and compressive strength tests were limited to two each for the parallel-to-centerline portion of the cured insert. All obtainable test values were normal and acceptable.

The test ring for the perpendicular-to-centerline carbon portion of the insert was destroyed by machining. Available material from the forward inside corner of the billet showed acceptable physical properties but insufficient material was available for mechanical properties tests (SDAR 34311).

Radiographic inspection prior to and visual inspection after final machining of the nose insert revealed two holes drilled for thermocouples remained in the final part profile (SDAR 34332). The holes were approximately 1/8 and 1/16 inch in diameter, respectively, 180 degrees apart, nearly perpendicular to the nozzle centerline, and extended completely through the insert.

IV, C, Nozzle (cont'd)

The maximum depth of the holes relative to the nose station was approximately 0.15 in. Repair consisted of filling with graphite-loaded epoxy resin cured at ambient temperature. Filling was verified by radiographic inspection.

The sequence of fabrication of the submerged insert (P/N 1127945-5) is reversed from the usual operation, since the insert functions on an outside surface. The silica overwrap was laid up with gore patterns, preformed, and machined. The bias cut carbon and silica were wrapped at a starting angle of 88 degrees using the overwrap as the mandrel surface. The maximum predicted laminate orientation change during debulk was 10 degrees.

The physical and mechanical properties test results required by Process Specification AGC-36413C for the cured parts are summarized in Figures 18 and 19. Except where insufficient material was available from the test rings, all results were normal and acceptable.

4. Assembly

The ablative inserts were bonded in place using Shell Chemical Co. adhesive Epon 913 conforming to Specification AGC-34151, Type II, using an ambient temperature or optional 115°F cure cycle. The steel faying surfaces were prepared by application of Fuller 162-Y-22 epoxy primer conforming to Specification AGC-34345, Type II. As reported by SDAR-34325 and SDAR 34326, the bond lap-shear test samples consistently failed to meet Specification AGC-36497 requirements of at least 2700 psi average and 2300 psi minimum value. Average values ranged from 1596 to 2631 psi. The bond failures were cohesive within the primer. Since the test values are not consistent with

IV, C, Nozzle (cont'd)

previous history, the exact cause is not known. However, the test strengths indicated adequate structural capability. There were no discrepancies reported by ultrasonic inspection of the bond lines.

Final machining of the entrance contour was accomplished after completion of bonding of the entrance assembly components. Leak testing of the inserts and the final assembly was accomplished with a helium leak detector (in lieu of the specified halogen leak test) because of halogen indications originating from uncured components of the silicone rubber potting in the ablative joints. No leakage was detected. The nozzle assembly is shown after completion of fabrication in Figure 20.

After receipt of the nozzle at Solid Rocket Operations (SRO), Sacramento, the IBT-100 insulation was applied using an air-operated caulking gun (Figure 21), and troweled to the required contour of drawing 1128286. A 48-hr cure cycle completed this processing operation. Figure 22 shows the IBT-100 coverage during the first pass of the applicator.

The nozzle prefire contour was defined in accordance with Project Directive No. 307, Rev. 1, using three methods:

a.   Dimension measurement of stand-off between the nozzle surface and a specially fabricated template (T-1018861).

b.   Radial measurements on a rotating surface table.

c.   Tangential radiographic exposures.

As a result of the radiographic inspection, it was discovered that a separation of approximately 0.024 in. existed between the mating faces

IV, C, Nozzle (cont'd)

of the nozzle shell-to-entrance ring O-ring seal joint. Apparently, improper procedures during the assembly dry fit of the threaded joint prevented positive verification of seating of the joint during final assembly. The 0.024-in. separation would not allow proper compression of the O-ring, therefore, the motor leak test was repeated using a modified leak test closure which plugged the nozzle at the throat, rather than at the exit plane. No leakage was detected at 50 psi internal pressure, thus verifying the integrity of the defective joint.

D. IGNITION SYSTEM

260-SL ignition motor booster, S/N 260-IMB-07, was the last remaining unit manufactured for the 260-SL-1 and -2 Motor Demonstration program. Thirteen boosters had been manufactured, twelve of which had been successfully test fired. Unit 260-IMB-07 had been designated as a spare and stored at the Aerojet-Dade Division.

When the unit was returned to the igniter processing line at the Sacramento Plant, the 1400 gram main charge, P/N 600269-9, and the 78 gram primary charge, P/N P1971274, were removed from the 260-SL ignition motor adapter assembly. The components were visually inspected to verify the structural integrity of the pyrotechnic Alclo-Iron grains. The pyrotechnic units were assembled to the mounting adapter, P/N 1128281-1. Following this assembly, 2.0 grams of Alclo pyrotechnic powder were loaded in the adapter cavity and the PE-451-003 power cartridge was installed. The exposed portion of the igniter adapter was insulated with NT-1001 trowelable insulation. The

IV, D, Ignition System (cont'd)

completed igniter was returned to its original shipping container and stored in a controlled environment magazine until final assembly in motor 44-SS-4.

E. FINAL ASSEMBLY

1. Pre-Assembly Inspections

On arrival at Sacramento, motor 44-SS-4 was visually inspected for evidence of damage that could have occurred during overland shipment from Aerojet-Dade Division. No damage was detected and the motor was released for further processing.

A radiographic inspection of the chamber and grain assembly was conducted to verify the acceptability of the grain, liner, and insulation system. The results of this inspection were as follows:

a. Approximately 30 small, isolated voids were present in the grain, with no obvious pattern relationship which could cause abnormal flame front advance.

b. There were four locations of questionable bond integrity between the chamber insulator and the case. All these areas were surrounded by suitably bonded material and no gas path to the chamber wall existed.

c. Propellant bonding to the liner was very good and the release boots were well bonded to the insulation over the prescribed length at the cylindrical section. They were released or unbonded on the head sections.

It was concluded from the radiographic inspection that the chamber and grain assembly were free of any detrimental condition which could compromise success of the static test firing.

IV, E, Final Assembly (cont'd)

2. Igniter Installation

The igniter, P/N 1128284-9, was installed with the motor secured in the vertical position, nozzle end up. The igniter was lowered into position through the aft end of the motor using special insertion tool T-1004510. O-rings, retaining ring 1128282-1, and a snap ring were installed in accordance with the requirements of Drawing 1128287. Sealant material 1913-4 was substituted for the specified AGC-34076 Class 5 (PR-1910-8) when laboratory tests determined that the material would not cure. Dimensional measurements were taken of the clearance between the forward face of the retaining ring and the igniter adapter before and after assembly to verify the retaining ring was fully engaged and seated against the mating adapter face.

3. Nozzle Installation

Prior to installation of the nozzle on the motor, the pre-fire contour was established as previously described.

The nozzle assembly was accomplished without difficulty with the motor in the vertical position, aft-end up. A dry-run fit was

IV, E, Final Assembly (cont'd)

first conducted using witness putty to define the gap dimensions at the chamber-to-nozzle insulation interface and between the aft-grain restrictor and nozzle insulation. Sealant material PR-1913-4 was then applied to these areas to a thickness slightly greater than the measured gap. PR-1913-4 was used instead of the PR-1910-8 required by Drawing 112827 as discussed in the preceding section.

The final installation of the nozzle was completed in accordance with Drawing 1128287.

4. Leak Test

When motor assembly had been completed, two pressure transducers were installed on the igniter adapter and the motor was leak tested. The chamber interior was pressurized to 50 psig, using a nitrogen and Freon gas mixture. All seal interfaces were checked with a Halogen leak detector unit and Leak-Tek solution; no leaks were detected. A second leak test was conducted to verify joint seal integrity between the nozzle throat and throat extension insert. This test, discussed in Section IV.C.4., demonstrated the acceptability of the assembled motor.

5. Retaining Ring Insulation

Application of the AGC-34335, Type I (V-61) insulation to the nozzle aft retaining ring completed the motor assembly procedure. The V-61 was cured for 5-1/2 days, instead of the 7 days required by the material specification. However, an average Shore D hardness of 28.5 was measured (38 is the specification lower limit), which was considered acceptable for the material's intended function of protecting the retaining ring bolts.

IV, E, Final Assembly (cont'd)

6. Motor and Component Weights

During motor and component processing, accurate weight records were maintained and are summarized in Figure 23.

V. TESTING

A. TEST SETUP

The motor was fired in the horizontal attitude in Test Stand W-2 of the Solid Rocket Test Area. The motor was mounted in a Minuteman second-stage motor ballistic firing fixture (T-407411). An existing Minuteman thrust tripod was modified to increase its structural strength and an axial flexure (P/N 1018533-201) was fabricated to transmit the motor thrust to the load cell. A quench tool, consisting of a hydraulic powered arm containing multiple spray heads, was positioned to permit rotation into the nozzle. This system directs a water fog spray against the nozzle ablative inserts (aft of the nose) and a heavy stream directly into the motor. A portable temperature conditioning house was placed over the entire test setup until T-3, and a temperature of $80 \pm 5°F$ was maintained during all test preparations. The motor is shown ready for static testing in Figures 24 through 26.

B. INSTRUMENTATION

Instrumentation consisted of two pressure transducers mounted on the igniter adapter, a load cell for measuring the axial thrust, and 12 thermocouples on the nozzle shell. The thermocouples were spot-welded to the shell opposite the location of maximum expected erosion of the nozzle insulator. All data were recorded on a Beckman Model 210 Analog-to-Digital Converter (ADC)

V, B, Instrumentation (cont'd)

and recording system. Ballistic parameters were also recorded on a CEC Model 5-119 oscillograph. The load measuring system, pressure transducer arrangement, and a typical thermocouple installation are shown in Figures 27 and 28. A summary of the sensing instruments used is listed below: '

Parameter	Instrument	Model	Range
Chamber Pressure	Pressure Transducer	Tabor Model 206	0-750 psig
Thrust	Load Cell	Baldwin-Lima-Hamilton &U3XXA	0-200K
Temperature	Thermocouples	Chromel-Alumel	0-500°F

Indications were also recorded of fire-switch actuation, EBW firing unit discharge and quench boom rotation command. Three motion picture cameras documented the test firing. The cameras were loaded with color film and the framing speed set at 500 fps (2 cameras) and 64 fps (1 camera). They were located so as to provide optimum coverage for malfunction analysis.

C.   DATA REDUCTION AND ANALYSIS

Data recorded in digital form on magnetic tape, as obtained from the ADC system, were reduced by a series of computer programs that apply the calibration factors to each channel and convert electrical counts to pressure, thrust or temperature values. An output tape and a tabulation are produced from these programs. This tape was in turn used as the input to a ballistic analysis program (No. 604, Part I) processed on an IBM 360/40 computer. This program accomplishes an averaging of pressure and thrust channels, converts psig to stagnation pressure in psia, provides an instantaneous integral of pressure and thrust, and calculates the apparent nozzle throat vs. time at two preselected efficiency levels (K_F).

V, C, Data Reduction and Analysis (cont'd)

Knowing the actual pre- and post-test throat area, a K_F value was selected which best fit between the two computer calculated K_F curves and the data was processed through Part II of the 604 program. This part of the program calculates the instantaneous throat area, C_F, mass flow and specific impulse at motor and standard conditions.* The output of this program was a tabulated summary of the above data and an X-Y plot of pressure, thrust and throat area vs. time.

D.   TEST PROCEDURE

The test firing procedure for motor 44-SS-4 was relatively simple and straight forward. After the motor was secured and aligned in the test fixture, the thrust-tripod, flexure, and load cell assembly were installed. Positioning and bolting of the flight retention and quench tooling to the test stand decking completed the mechanical setup.

Installation of the 12 thermocouples on the nozzle and ranging and calibration of ballistic data channels on the end recorders was completed concurrently with the mechanical preparations.

All terminal countdown functions were initiated automatically by the firing programmer. At the firing command, 2000 vdc was discharged from a 0.5 to 1.0 microfarad capacitor to the EBW squib of the igniter. Quench system actuation was manually initiated when chamber pressure was approximately 1.5 psig.

Following the test, the operations below were completed:

1.   The fired chamber was removed from the test stand and all residual quench water drained out.

---

*$I_s(\text{std}) = I_s(\text{mc})$ adjusted for 1000 psia chamber pressure, 14.7 ambient pressure, 15 degree half-angle and optimum expansion ratio.

V, D, Test Procedure (cont'd)

    2.   A 72 hour drying cycle at +180°F was performed.

    3.   The nozzle was disassembled from the chamber and profile measurements made in the same manner as before the test.

    4.   Rubber molds were made at various locations in the submerged section of the nozzle.

    5.   The nozzle was sectioned at 0 and 300 degrees for further performance evaluation.

    6.   Complete reduction and analysis of ballistic data was conducted.

VI.   TEST RESULTS

Subscale motor 44-SS-4 was successfully static test fired on 22 March 1967. Motor performance was normal over the entire duration and all components were in excellent condition after the test.

There was no loss of any recorded parameter and the quality of reduced data was good. The variation between the two channels of measured thrust was less than 0.005% at maximum thrust. Operation of all test systems was normal. A time-event summary of the test sequence is shown in Figure 29.

Temperature data monitored on the nozzle shell showed a nominal increase of 10 to 15°F above ambient air temperature. As these measurements were primarily for malfunction analysis, and data indicates no heat transfer through the insulation to the shell, the results will not be discussed further in this report.

The ballistic and component performance evaluation and analysis are discussed in the following sections.

VI. TEST RESULTS

A. IGNITION PERFORMANCE

Ignition of motor 44-SS-4 was satisfactory; the ignition transient is shown in Figure 30. Ignition interval occurred 0.052 sec after capacitor discharge to the EBW power cartridge. Because of the higher than required available igniter energy and the igniter burning duration (100 millisec), a 15 psi overpressure occurred for approximately 40 millisec after the motor attained initial steady state operating pressure.

B. BALLISTIC PERFORMANCE ANALYSIS

The measured motor 44-SS-4 chamber pressure- and thrust-vst-time performance curves are shown in Figure 31. A summary of the motor ballistic performance characteristics is given in Figure 32. The operation was normal, with no indication of any performance anomalies. The standard specific impulse obtained in the firing was 244.7 lbf-sec/lbm, which corresponds closely to the average value of 244.4 lbf-sec/lbm obtained in the three previous 44-SS motor firings. As expected, the submerged nozzle entrance configuration did not result in a detectable performance loss, as compared with earlier convergent nozzle entrance configurations.

The comparison between the pre-firing chamber pressure-vs-time performance prediction and the actual measured pressure-vs-time curve is shown in Figure 33. While the predicted and actual curve shapes are quite similar, the actual chamber pressure was significantly higher and the web action time shorter than predicted. It is evident that the propellant burning rate in motor 44-SS-4 was somewhat higher than predicted.

VI, Test Results (cont'd)

The pre-firing performance prediction was obtained using the Aerojet ballistic Computer Program 1103, and was based on the 3KS-500-size motor burning rate data obtained from the two batches of propellant cast in motor 44-SS-4. No scale-up in burning rate was anticipated from 3KS-500-size motors to the 44-SS size motor, since little or no scale-up had been observed in previous 44-SS motor firings. However, the previous 44-SS motors used ANB-3105 propellant, rather than the higher burning rate ANB-3254 formulation. It appears that the changes made in achieving the increased ANB-3254 burning rate caused a change in scale-up behavior.

Analysis of the motor 44-SS-4 performance indicates that the effective propellant burning rate was about 3.6% higher than that used in the performance prediction. Subsequent to the firing, a computer performance run was made using a burning rate 3.6% higher than was applied in the predicted performance calculations. The resulting pressure-vs-time curve is shown in Figure 34, compared with the actual measured pressure for motor 44-SS-4. The analytical result, using the adjusted burning rate information is in close agreement with the actual motor performance. The occurrence of this burning rate scale-up will be taken into account in the assessment of burning rate data from the 260-SL-3 motor propellant batches, and in the prediction of the motor 260-SL-3 performance.

C. COMPONENT EVALUATION

1. Chamber and Insulation

The internal insulation performance in the previous 44-SS motors, which burned 8 to 10 sec longer than motor 44-SS-4, showed no

VI, C, Component Evaluation (cont'd)

indications of excessive erosion. Because of the short burning duration of
motor 44-SS-4, no qualitative post-fire measurements were taken on the internal
insulation. A visual inspection of the internal insulation revealed that the
forward and aft boots were still intact and showed very little effect from heat.
There were no marginal performance areas or visual discolorations on the chamber
exterior. A post-fire view of the chamber interior is shown in Figure 35.

2. Aft-Grain Restriction

As may be seen from the postfiring view (Figure 36) the IBT-106
grain restriction was in excellent condition after the test. The oscillograph
record of the firing indicates that propellant-to-restriction bond integrity
was maintained over the full test duration. There was no evidence of hot-gas
penetration past the PR-1913-4 seal on the back side of the restriction.

The exposed interior surface of the restrictor was covered with
a heavy, relatively hard char, ranging from approximately 0.07 to 0.19-in. thick.
At the locations of maximum impingement in line with the grain valleys, (0, 120
and 240 degrees) and where nearly 12 sec of exposure occurred, approximately
0.08-in. of uncharred material remained of the original 0.388-in. nominal
thickness. Figure 37 shows a cross-section through the restriction and
summarizes material loss data at the area of maximum erosion. IBT-106 was
demonstrated to be very effective as an insulator and restriction material.
The relative ease of processing and application make IBT-106 attractive for
use on future large solid rocket motors.

VI, C, Component Evaluation (cont'd)

     3.   Nozzle

        a.   Nozzle Shell Insulation

           The maximum measured rubber thickness losses in the

nozzle shell are summarized in the following table:

Station (Station Location Shown in Fig. 38)	Approx. Dia, at Steel Surface, in-dia	Area Ratio	Mach No	Maximum Measured Thickness Loss, in.	Thickness Loss Rate*, in/sec
2	24.7	2.5	0.24	0.44	0.036
3	26.1	2.8	0.22	0.62	0.051
4	27.5	3.2	0.19	0.45	0.037
5	29.1	3.5	0.17	0.34	0.028

*Determined as the maximum thickness loss
 divided by the web burning duration, 12.1 sec.

The design data relating Gen-Gard V-44 thickness loss rate to gas velocity (Mach

number) is shown in Figure 39; included in this figure are the rubber thickness

loss rates experienced in the 260-SL motors and motor 44-SS-4. The data points

at Stations 3, 4 and 5 closely follow the established design values. The erosion

at Station 6 is understandably much lower than would be expected at this area

ratio. Since this station is only 0.13-in. aft of the aft propellant and re-

striction face, the rubber was not exposed directly to high velocity gas flow

until some indeterminate time after ignition. Erosion at Station 2 indicates

this area is near to or in the stagnation region previously observed in submerged

nozzle applications and, therefore, did not experience high velocity flow.

           The overall nozzle shell insulation erosion pattern is

shown in Figure 40. The maximum erosion at Stations 3, 4 and 5 occurs coincident

VI, C, Component Evaluation (cont'd)

with the valleys in the propellant grain configuration. The maximum erosion pattern at Station 2 also is coincident with the grain configuration valleys, but not to the extent shown in the higher erosion areas.

Due to the limited access area, highly accurate measurements of IBT-100 trowelable insulation thickness loss were not possible. The thickness loss data obtained by measuring the postfire standoff distance from the template used to trowel the IBT-100 material into place is shown in Figure 41. The difference in erosion patterns in the IBT-100 is shown graphically in Figure 41 (Sheet 2). This data was taken from tracings of rubber molds made every 60-degrees in the submerged section. Assuming a 12.1 sec exposure time, the maximum thickness loss rate was 0.028 in/sec. This value cannot be correlated to previous data since the gas velocity in this region is unknown.

Based on the observed rubber thickness loss rate in motor 44-SS-4, the apparent nozzle shell insulation safety factors at equivalent locations in motor 260-SL-3 are presented in Figure 42.

b. Plastic Inserts

The nozzle assembly performed successfully throughout the motor firing. The primary objective of the test, to obtain nozzle material performance data to confirm the 260-SL-3 nozzle design, was accomplished.

(1) Erosion Performance

Pretest and posttest measurements were taken of the nozzle ablation surfaces to provide data for analysis of the erosion characteristics. Loose char was removed from the rubber insulation surfaces prior

VI, C, Component Evaluation (cont'd)

to the posttest measurements. Measurements were obtained at six equal, radial locations, starting at the 0 degree orientation. These locations corresponded to the three star points and the three star valleys of the propellant grain configuration. For each radial location, standoff distances were measured from an inspection template at axial stations that provided a comparison with predicted erosion from heat transfer analysis. Differences in standoff distance between pretest and posttest measurements provided the actual erosion depths for comparison.

In addition, radial dimensions and X-ray photographs were taken before and after test at the same radial locations to verify the erosion data obtained from template measurements. Some disparity was observed between the radial measurements and the other data. This was apparently caused by the incompatibility of the inspection tool with the surface roughness.

Erosion profiles of the nozzle submerged cavity were obtained by rubber molds. Silicone rubber was cast in the cavity at the selected radial locations and subsequently removed to determine the actual contour. These erosion profiles compared closely with the contours obtained from the X-ray photographs.

By comparatively evaluating the measurements obtained from the various inspection methods, a set of resultant data, which could be confirmed by more than one inspection method, was obtained. A summary of the resultant erosion depths at various stations of the nozzle is shown in Figure 43. Erosion depths are tabulated for the six radial locations and the

VI, C, Component Evaluation (cont'd)

average erosion is included for comparison with the predicted erosion depths. A curve of depth versus nozzle station from the nose section to the exit plane is shown in Figure 44.

The erosion performance of all nozzle materials was within design limits, which were based on twice the predicted recession depth. At the throat, the average recession depth was 0.04 compared with a predicted depth of 0.07 in. At all other stations of the nozzle, except the nose station, the average recession depths were lower than predicted. The probable cause for the overprediction is attributed, at least in part, to a net growth within the char layer of the material. This growth is confirmed by posttest measurements which indicated that negative erosion, or material growth existed in the carbon cloth portion of the submerged insert and in the nozzle expansion section between area ratios of 1.60 and 2.46. The physical explanation of this phenomenon is not established, but the growth is seemingly more pronounced on lesser angles of laminate orientation as evidence from previous nozzle tests. Possible explanations for the char layer growth include high cross-ply thermal expansion exists at the char temperature, high internal pressure due to pyrolysis of gas generation, or movement due to rapid cooling at shutdown.

Other factors, which might contribute to the overprediction for this nozzle included the effects of a short duration test. From the ballistic performance data of this motor, negligible throat area change was observed for the initial four sec of the motor test. This time

VI, C, Component Evaluation (cont'd)

interval corresponds to nearly one-third of the motor duration. Since the predicted erosion depths are based on average recession rates for the full motor duration, overprediction of the nozzle erosion depth will result.

As shown in Figure 44, the profile of measured erosion depths is compared with the predicted material loss. The most pronounced difference was at the nozzle entrance section between the nose (ϵ = 2.00) and throat (ϵ = 1.00) stations. The predicted erosion profile was determined using cold flow test data* in the heat transfer analysis.

Results of cold flow test indicated that the Mach number for the propellant star point location is higher than the grain valley location at the nose station, but rapidly drops lower than the grain valley location downstream from the nose station. The effect is caused by circumferential flow from the grain valley to the star point locations observed in the submerged cavity. Therefore, maximum erosion was predicted to occur near the nose station for the propellant grain valley location and near the throat station for the star point location.

Maximum measured erosion for both propellant star point and grain valley locations existed at the nose station. The erosion at the nose station for star point locations was 0.06 in. and was the same as predicted. Since more particle impingement and higher mass flow emerges into the nozzle at the propellant grain valley, higher nozzle erosion at these locations was, therefore, expected. The profile of measured nozzle erosion

---

*NASA conducted cold flow program on a 260-SL-3 subscale model "Mach Number Behind the Nozzle Entrance Section."

VI, C, Component Evaluation (cont'd)

showed that maximum erosion at the grain valley was 0.15 in., which was sub-stantially higher than at the star point locations. The maximum deviation of erosion depth from the predicted was at the nose station, where the average erosion depth was 0.10 in. compared with 0.06 in. predicted.

Erosion profiles of the submerged cavity revealed relatively uniform circumferential erosion within the grain valley locations, but the erosion was generally less at the propellant star point locations. Local circumferential waveness at the bottom of the cavity was observed on the IBT-100 insulation erosion surface near the 60, 180, and 300-degree locations, which corresponded to the propellant star points. The erosion pattern indicated a convergence of gas flow from two grain valley regions and subsequent turning of the flow into the nozzle at these locations. From the test results, it can be concluded that the primary gas flow in the cavity is axial, but circumferential flow from the grain valley to the star point locations did exist.

The erosion data of this nozzle test has been used to determine a revised Mach number distribution along the nozzle wall and to provide a more accurate erosion performance prediction for the 260-SL-3 nozzle. This analysis indicates positive safety margins exist throughout the nozzle and performance is expected to be satisfactory in all respects.

Circumferential variations in erosion are shown in Figure 45, and are plotted for four stations of the nozzle entrance section from the nose station to the throat. The scale of the erosion depths was enlarged to show the significance of the difference in depths. As expected, an erosion

VI, C, Component Evaluation (cont'd)

pattern existed which is caused by unsymmetrical gas flow from the propellant grain configuration. In all cases, higher erosion was observed at the three radial locations that correspond to the star valleys of the propellant grain, where the main mass flow was concentrated. Differences in erosion depths in the circumferential direction was a maximum of 0.12 in. at the nose station and decreased to 0.02 in. at the throat. This variation was not noticeable downstream from the throat.

The erosion surface upstream of the nozzle throat was generally smooth and uniform as shown in Figure 46. Some longitudinal waviness was seen on the surface of the throat extension insert as shown in Figure 47. These waviness are related to non-uniformity in the laminate orientation within the part and are discussed in the following section.

b.   Char Thickness and Structural Integrity

After firing, sections of the nozzle were removed to examine the char thickness, laminate orientation, and joint integrity. Two longitudinal cross-sections of the nozzle, including the steel shell, were obtained from the zero-degree and 300-degree radial locations. The zero-degree section, which is shown in Figure 48, is in the sector of the nozzle that was quenched with water.

The quench system directed a fine water spray on the nozzle interior from the nose to the exit plane and filled the horizontally positioned motor with water from burnout time until water flowed from the nozzle throat. With this method, only the bottom sector of the nozzle submerged section was quenched. The time interval from end of motor action-time to initiation of motor quench was 8.6 sec.

VI, C, Component Evaluation (cont'd)

Comparison between the zero-degree section and the 300-degree section, which was not deluged, did not reveal any appreciable differences in char thickness. This indicated that char growth due to heat soak was essentially completed prior to actual quenching of the nozzle or that steam generated by the water quench effectively terminated the charring action.

The average char thicknesses measured from these two stations are tabulated in Figure 49. Comparison with predicted char indicated that the measured thicknesses are higher at all stations of the nozzle. The difference was primarily attributed to additional char growth due to heat soak, since the predicted char thickness is based on motor burnout time. Heat transfer analysis of the throat station predicted that char formation continues after motor burnout as shown in Figure 50. The full char thickness including heat soak is predicted to be 0.35 in. and compared closely with the measured char of 0.32 in.

Significant differences in char thicknesses existed at the nose station, where the measured char thickness was 0.43 in. compared with a predicted thickness of 0.23 in. This difference is the result of two factors which were not included in the heat transfer analysis; variation of thermal conductivity with laminate orientation and the radius effect. Recent elevated temperature data* for MX-4926 carbon cloth phenolic showed that the charred

---

*NASA CR-72080, Aerotherm Report No. 66-2, Studies of Nozzle Ablative
 Material Performance for Large Solid Boosters, Page 12

VI, C, Component Evaluation (cont'd)

material thermal conductivity in the parallel to laminate direction is 1.7 times the conductivity in the perpendicular to laminate direction. An average value of thermal conductivity was used for the heat transfer analysis of this nozzle. Additionally, the small radius of curvature relative to the char thickness on the nozzle nose resulted in much higher heat input for a given volume of material than for a flat surface assumption which was used in the heat transfer analysis.

A revised heat transfer analysis of the 260-SL-3 nozzle design was conducted that included the consideration of these two factors in the prediction of char layer thicknesses. The effect of the radius of curvature is not significant on the 260-SL-3 nozzle design, since the nose radius is large compared to the char layer and the heat input approaches the flat plate analysis currently used.

The laminate orientation in the nozzle components are shown in Figure 51. The orientation of laminates for the nose insert is uniform and is within design requirements. Some reorientation as a result of the debulk and cure cycles was seen in the throat, submerged, and throat extension inserts. The ply orientation in the throat insert was 45-degree to nozzle centerline at the forward end. The orientation gradually changed from 45 to 90-degree to the erosion surface toward the aft end. The ply orientation in the submerged insert has many changes in angles within each ply, which is caused by the complex wrapping surface used during fabrication of this part. The change in orientation for both the throat and submerged inserts was orderly and no significant variation in surface erosion was observed.

VI, C, Component Evaluation (cont'd)

The laminate orientation angle in the throat extension insert was within the design tolerance of 25 to 35 degrees. However, local laminate reorientation or wrinkling existed in the part and caused longitudinal waviness on the erosion surface. The magnitude of the waves was a maximum of 0.05 in. The variations on the erosion surface resulted in corresponding waviness in the char layer.
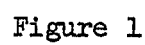
Some delaminations were observed from examination of the two cross sections of the nozzle. The majority of these delaminations cracks were found to extend only to the depth of the heat-affected zone. Those delaminations which extended to the surface of the overwrap showed no evidence of gas circulation or oxide deposit, and there was no indication of increased depth of the heat affected zone in the local area of the delamination.

Integrity of the joints between plastic components that are filled with silicone rubber sealant appeared excellent with no evidence of gas penetration into the steel components. The silicone rubber sealant was eroded away within the char layer thickness.

The interface joint between the nose insert and the submerged insert, which was bonded with Epon 913 epoxy adhesive, was separated to a width of 0.06 in. The adhesive was apparently eroded away during heat soak, but no evidence of gas penetration beyond the silica cloth overwrap was observed.

VI, C, Component Evaluation (cont'd)

The O-ring sealing surface at the threaded joint between
the entrance and shell assemblies was not in contact, which confirmed obser-
vations made of this condition from pretest X-ray photographs. An excellent
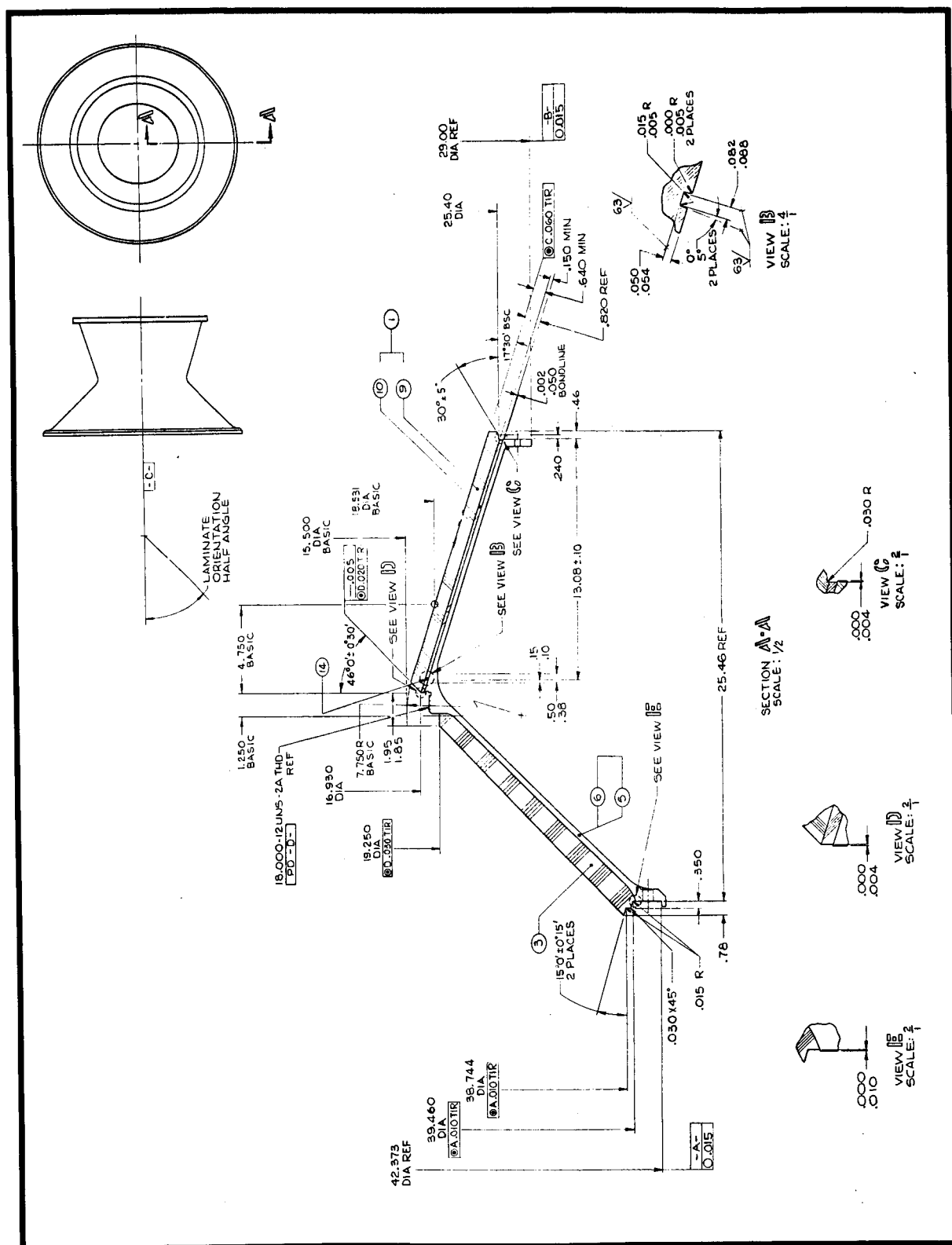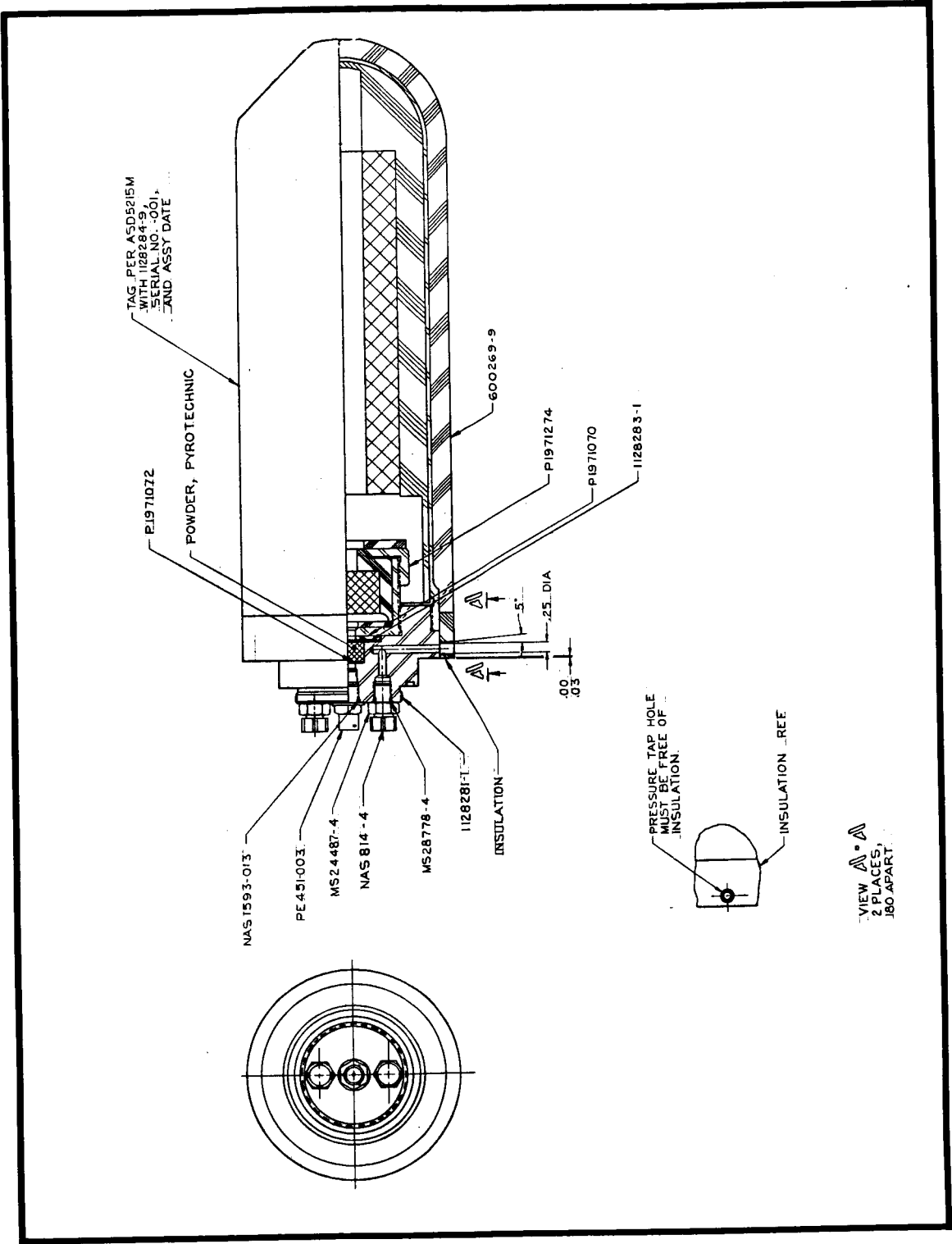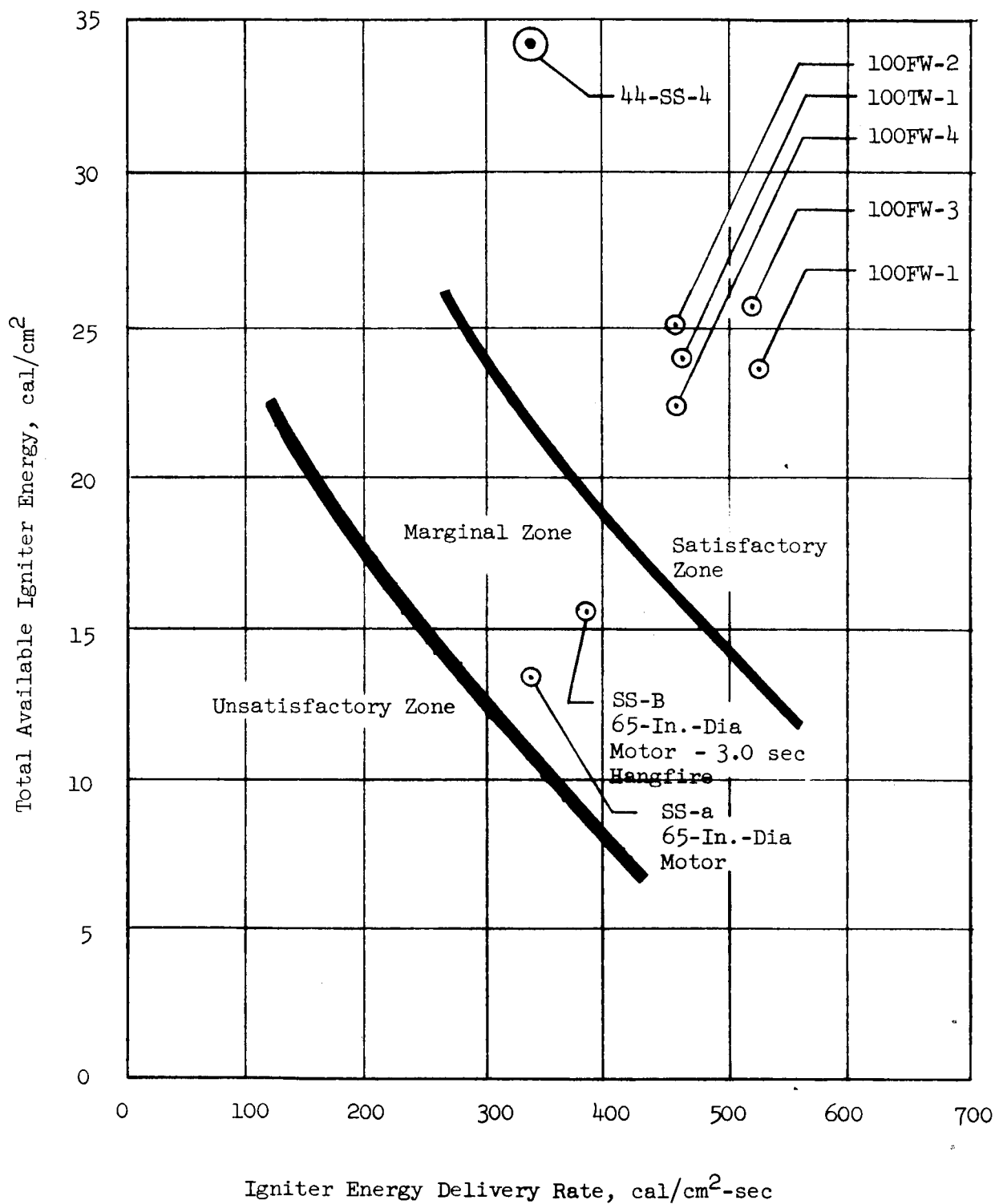redundant seal was provided by the IBT-100 trowelable insulation.

44-SS-4 Motor Assembly

Figure 1

Figure 2

44-SS-4 Propellant Grain

Nozzle Layout

Figure 3

Nozzle Shell Insulation

Figure 4

TAG PER ASD5215M
WITH 1128284-9,
SERIAL NO. -001,
AND ASSY DATE

PJ971072

POWDER, PYROTECHNIC

600269-9

PJ971274

PJ971070

1128283-1

.25 DIA

.5

.00
.03

NAS1593-013

PE451-003

MS24487-4

NAS 814-4

MS28778-4

1128281-1

INSULATION

PRESSURE TAP HOLE
MUST BE FREE OF
INSULATION.

INSULATION REF

VIEW △ - △
2 PLACES,
180 APART
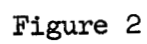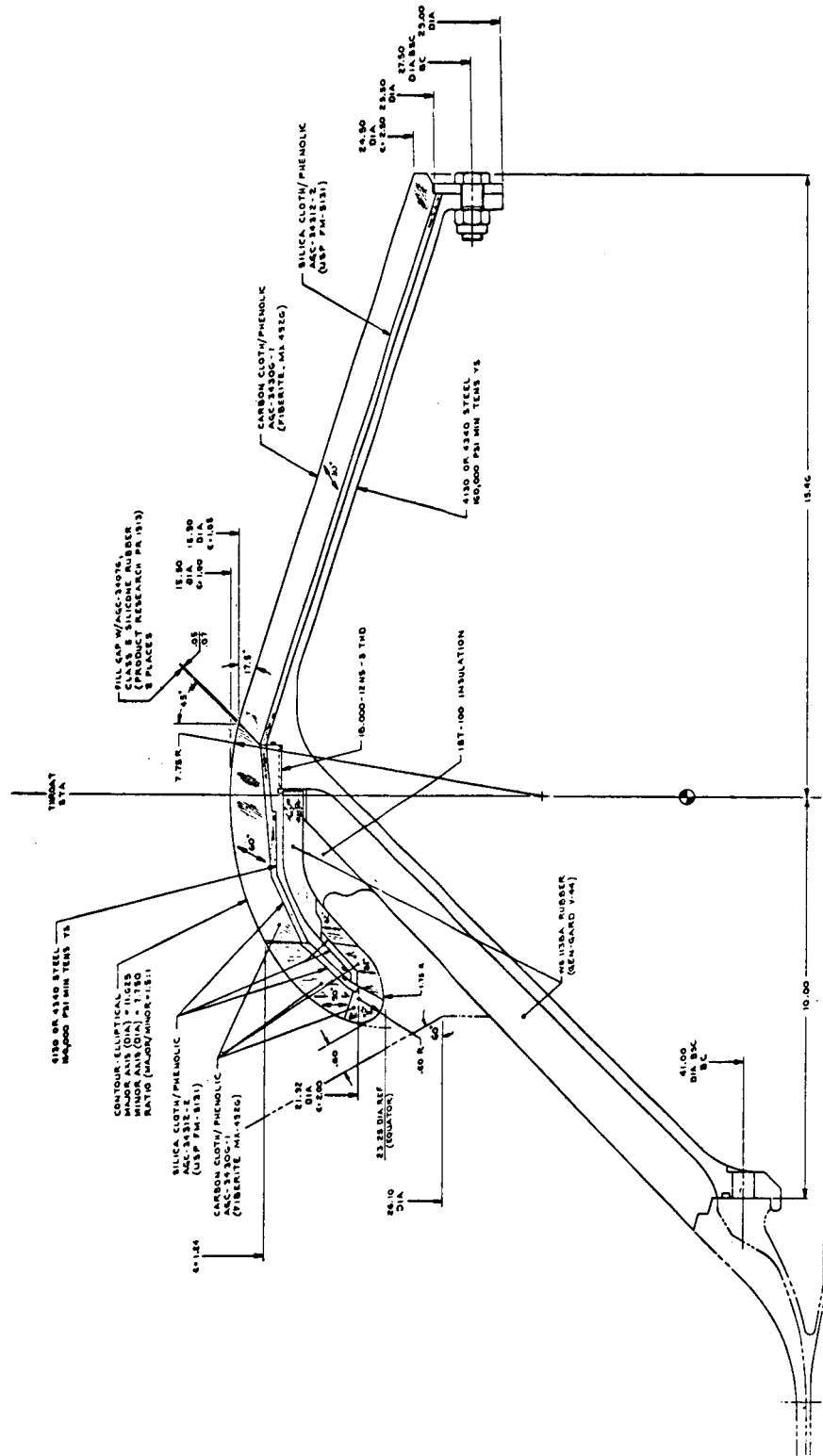
Igniter Assembly

Figure 5

Empirical Correlation of Igniter Energy Release Rates
for Various Motors

Figure 6

Lot 4 Material Qualification Run

Parameter	Acceptance Limits	Batch B-468	Batch B-469
Liquid Strand			
Burning Rate, in./sec	0.677 ± 0.030	0.680	0.698
		0.683	0.702
		0.679	0.702
		0.679	0.699
		$\overline{X}$ = 0.680	$\overline{X}$ = 0.700
Density; gm/cc	1.749 ± 0.007	1.748	1.748
Wt. % DER-332	1.23 ± 0.12	1.26	1.18

NOTE: All data are from samples taken at top of propellant pot.

44-SS-4 Propellant Acceptance Data

Figure 7

Batch No.	Cure Time, days	Mechanical Properties @ 77°F			
		S_{nm} (psi)	γ_m (%)	γ_b (%)	E_o (psi)
468	12	85	24	25	421
	16	101	26	28	509
	20	103	23	25	564
	24	108	25	26	582
	28	111	24	25	619
	32	112	22	24	631
469	12	92	23	24	506
	16	112	25	26	520
	20	101	21	22	565
	24	116	21	22	681
	28	112	22	23	642
	32	116	22	24	641
	40	124	19	19	780

Propellant Mechanical Properties vs Cure Time

Figure 8

Burning Rate

Batch	3KS-500 Motor Data r_b@ 600 psia (in/sec)
468	0.696
469	0.711
Lot 4 Qual. Average (6 batches)	0.706

Constant Strain Data

Batch	Applied Strain* (%)			
	10	15	20	25
468	2/2	2/2	2/2	-
469	2/2	2/2	2/2	1/2

*Bars holding/bars tested

(Propellant cured 24 days @ 135°F)

Burning Rate and Constant Strain Data
44-SS-4 Propellant

Figure 9
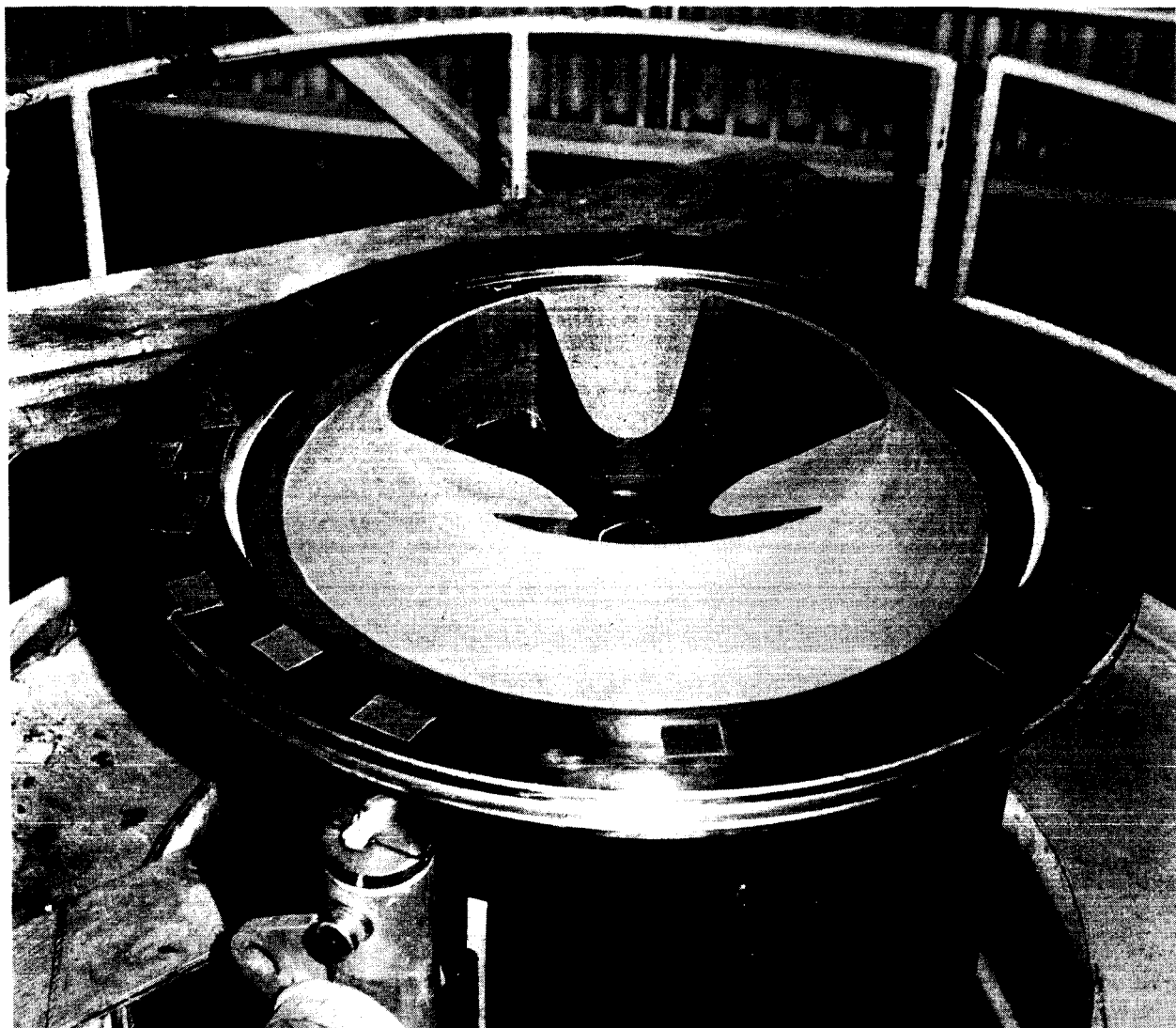
Trimmed Propellant Grain, 44-SS-4

Figure 10
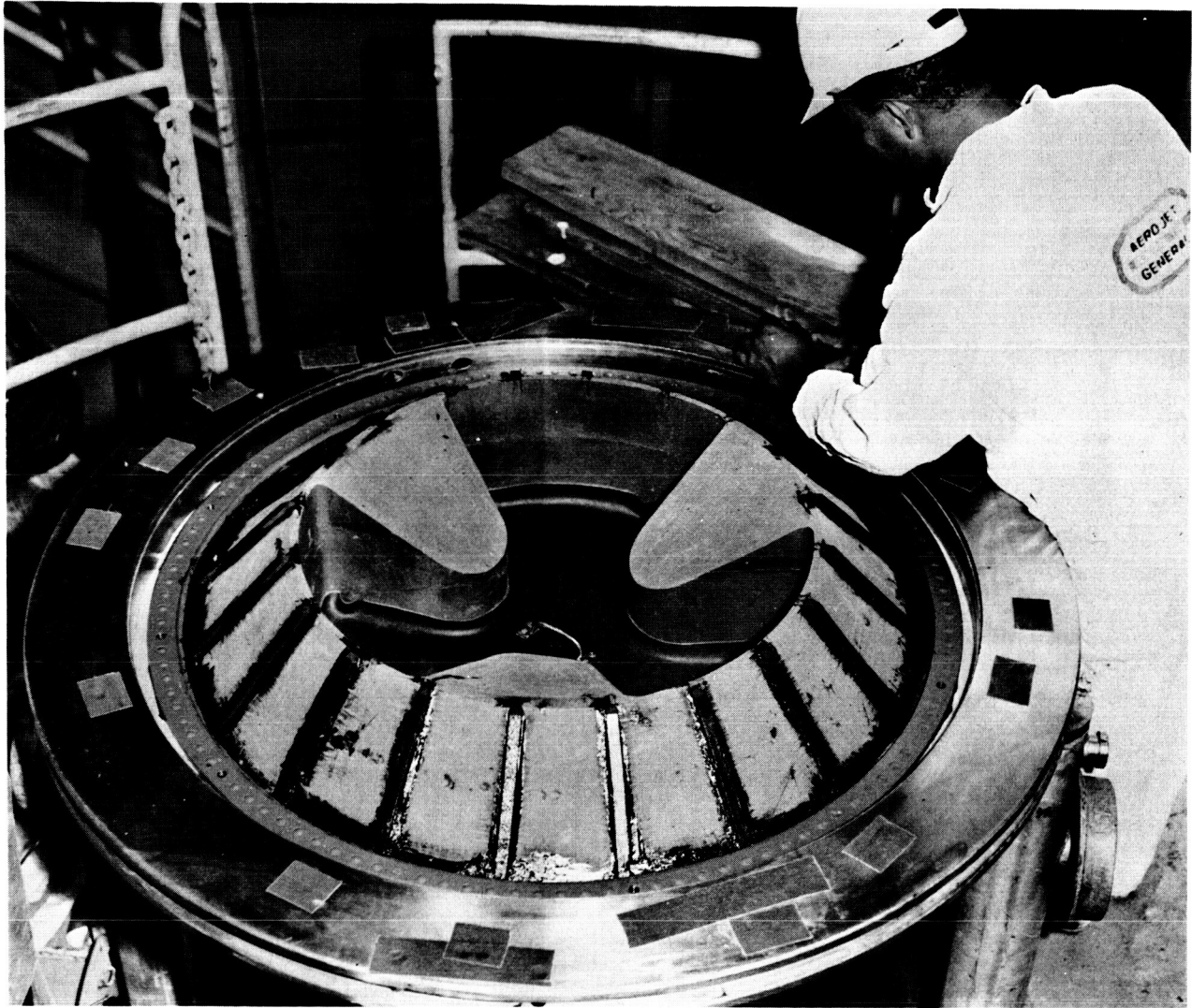
IBT-106 Guide Strips on Aft-Grain Face

Figure 11

44-SS-4 Grain After Completion of IBT-106 Application

Figure 13
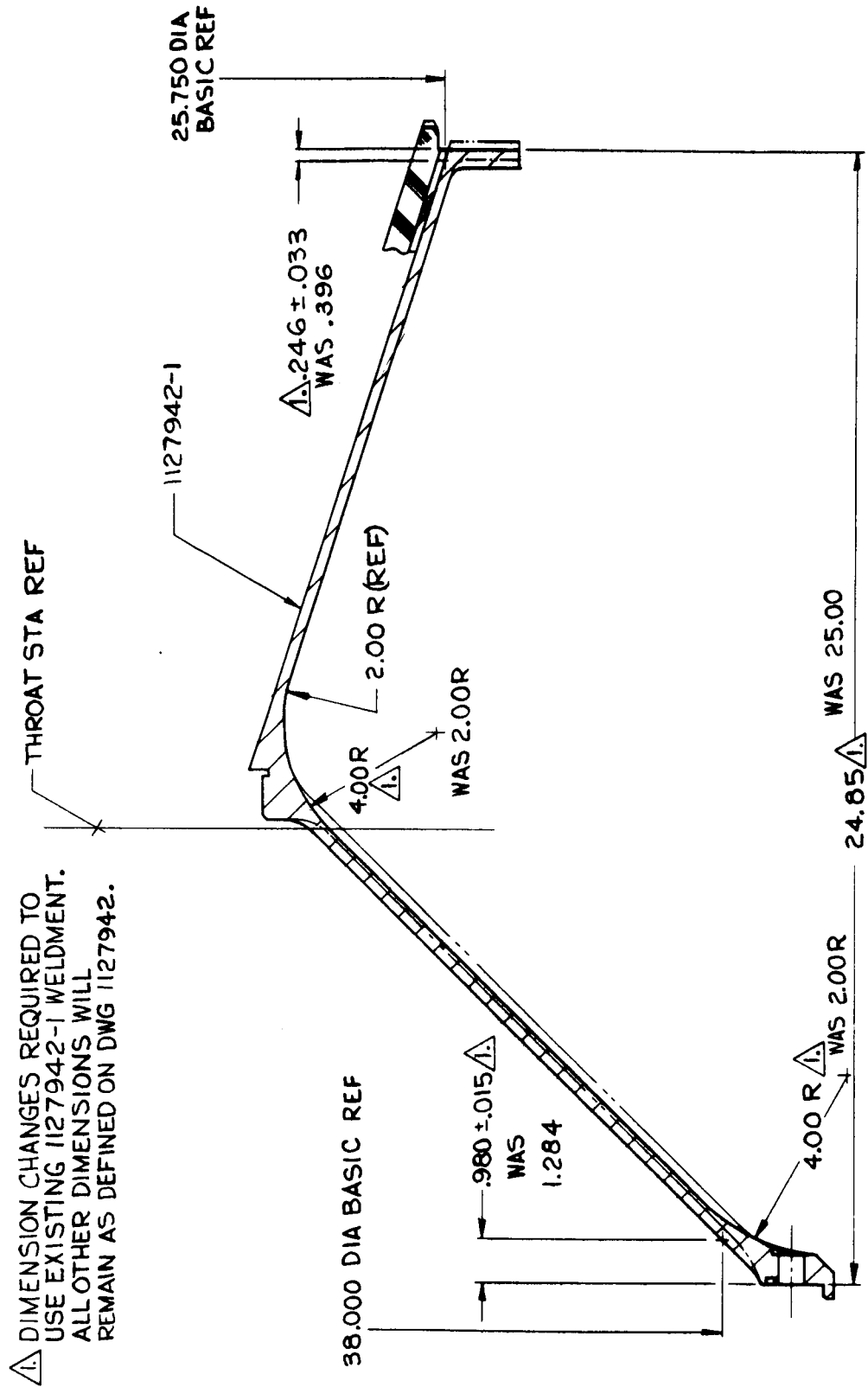
As-Built 44-SS-4 Nozzle Shell Configuration

Figure 14

44-SS-4 Nozzle Rubber Insulation Lay-Up

Figure 15

Throat Extension Insert Preparatory to Machining Overwrap

Figure 16
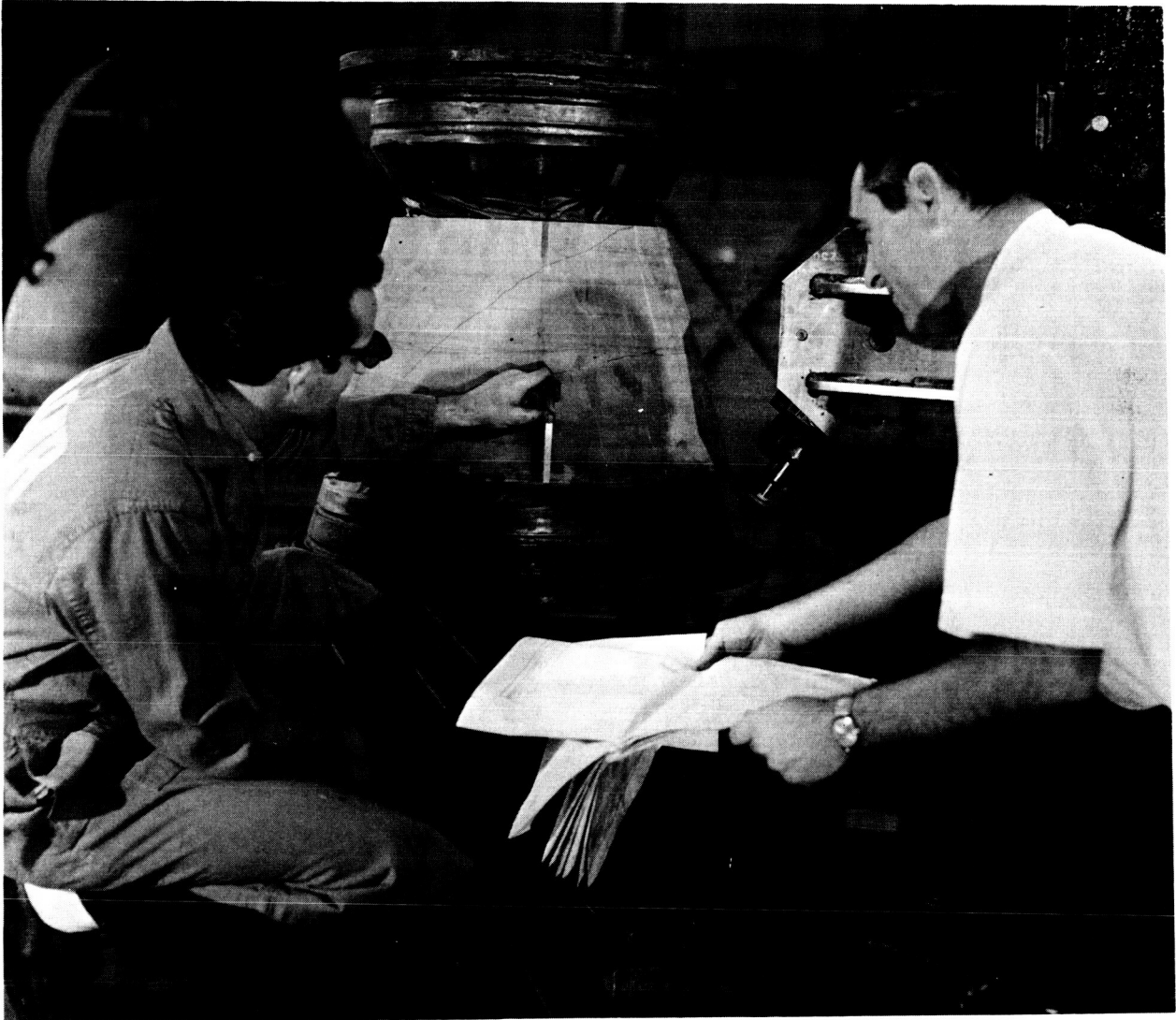
Machining of Submerged Insert

Figure 17

|	Specification AGC-35413 C Requirements	Throat Extension Insert 1127944-1	Throat Insert 1127945-1	Nose Insert 1127945-3 Bias Wrap	Nose Insert 1127945-3 Warp Wrap	Submerged Insert 1127945-5
Specific Gravity						
FTMS No. 406, Method 5011	1.38 min.	1.448	1.456	1.438	1.455	1.453
Volatile Content, wt%						
AGC-36413	3.0 max.	2.12	2.70	2.26	2.47	2.06
Acetone Extraction, wt%						
ASTM D494	1.0 max	0.52	0.78	0.24	0.22	0.102
Compressive Strength, psi						
FTMS No. 406, Method 1021	30,000 min.	33,968	33,563	32,738	**	33,544
Compressive Modulus, psi						
FTMS No. 406, Method 1021	Report	1.99×10^6	2.12×10^6	2.48×10^6	**	1.64×10^6
Interlaminar Shear Strength, psi						
FTMS No. 406, Method 1041	2,000 min*	5,815	6,187	6,849	**	4,448
Microtensile Strength, psi						
ASTM D 1708	Report	17,461	15,073	17,211	**	15,347

* Specification AGC-36413C requirement is based on FTMS No. 406, Method 1042, which normally yields results of approximately one-half of the magnitude of Method 1041 which was actually used.

**SDAR-34311 - Test ring erroneously machined. Insufficient material for test specimens.

Figure 18

Final Part Properties - MX-4926 Carbon Cloth (AGC-34306-1)

	Specification AGC-35413 C Requirement	Throat Extension Insert 1127944-1 Warp Wrap	Throat Insert 1127945-1 Bias Wrap	Nose Insert 1127945-3 Layup	Submerged Insert 1127945-5 Layup	Submerged Insert 1127945-5 Bias Wrap
Specific Gravity						
FTMS No. 406, Method 5011	1.70 min.	1.741	1.763	1.722	1.740	1.753
Volatile Content, wt%						
AGC-36413	3.0 max.	2.32	1.90	2.12	2.28	2.72
Acetone Extraction, wt%						
ASTM D 494	1.0 max.	0.30	0.30	0.26	0.20	0.23
Compressive Strength, psi						
FTMS No. 406, Method 1021	15,000 min.	19,009	22,028	22,672	20,901	17,450
Compressive Modulus, psi						
FTMS No. 406, Method 1021	Report	1.88×10^6	2.19×10^6	1.78×10^6	2.18×10^6	1.66×10^6
Interlaminar Shear Strength, psi						
FTMS No. 406, Method 1021	1,200 min*	3,536	3,157	3,158	3,545	3,691
Microtensile Strength, psi						
ASTM D 1708	Report	9,774	13,627	13,687	12,749	10,514

*Specification AGC-36413 C requirement is based on FTMS No. 406, Method 1042, which normally yields results of approximately one-half the magnitude of Method 1041, which was actually used.

Final Part Properties - FM 5131 Silica Cloth (AGC-34312-2)
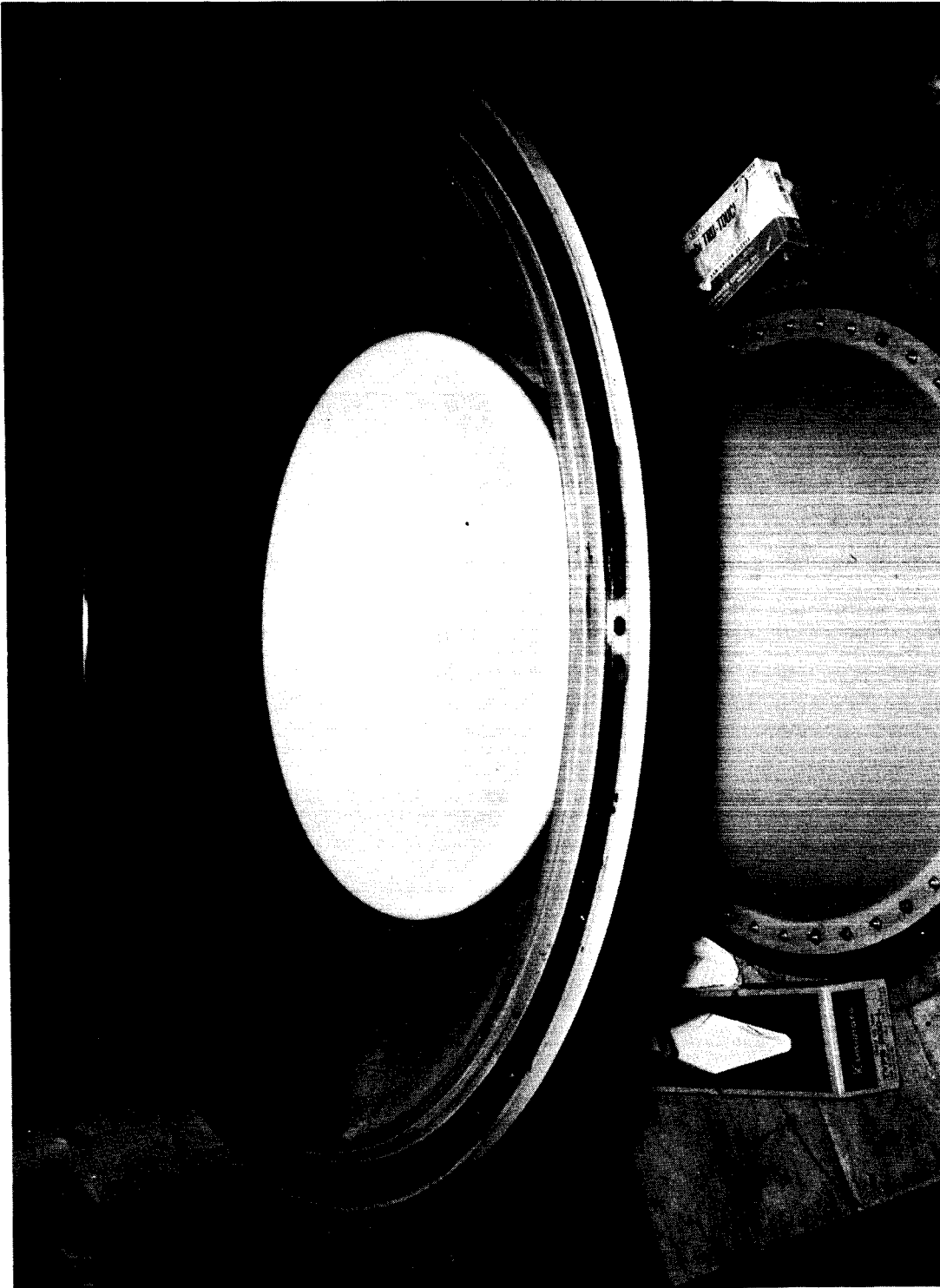
Figure 19

Completed 44-SS-4 Nozzle Assembly

Figure 20
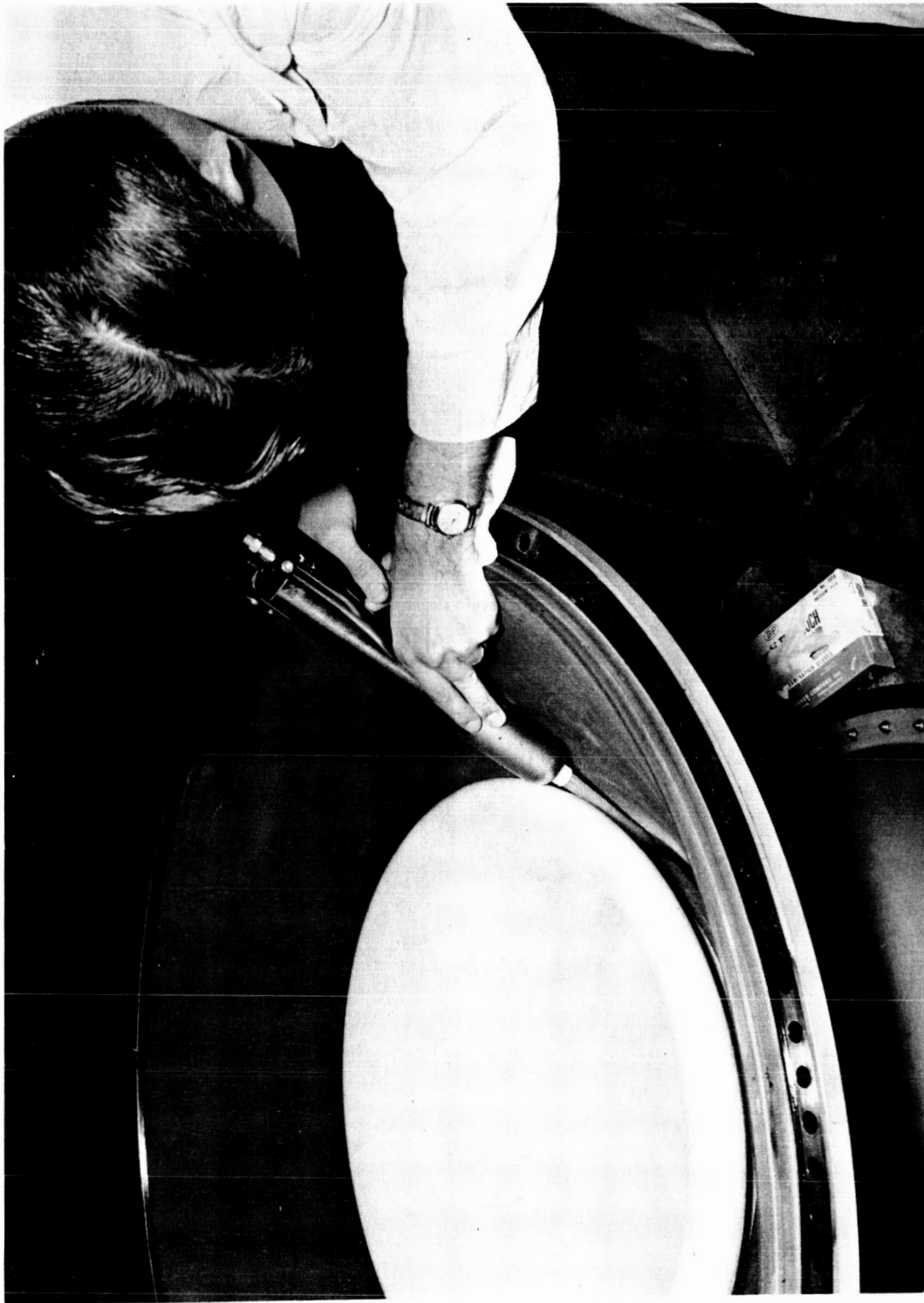
Application of IBT-100 Insulation to Nozzle

Figure 21
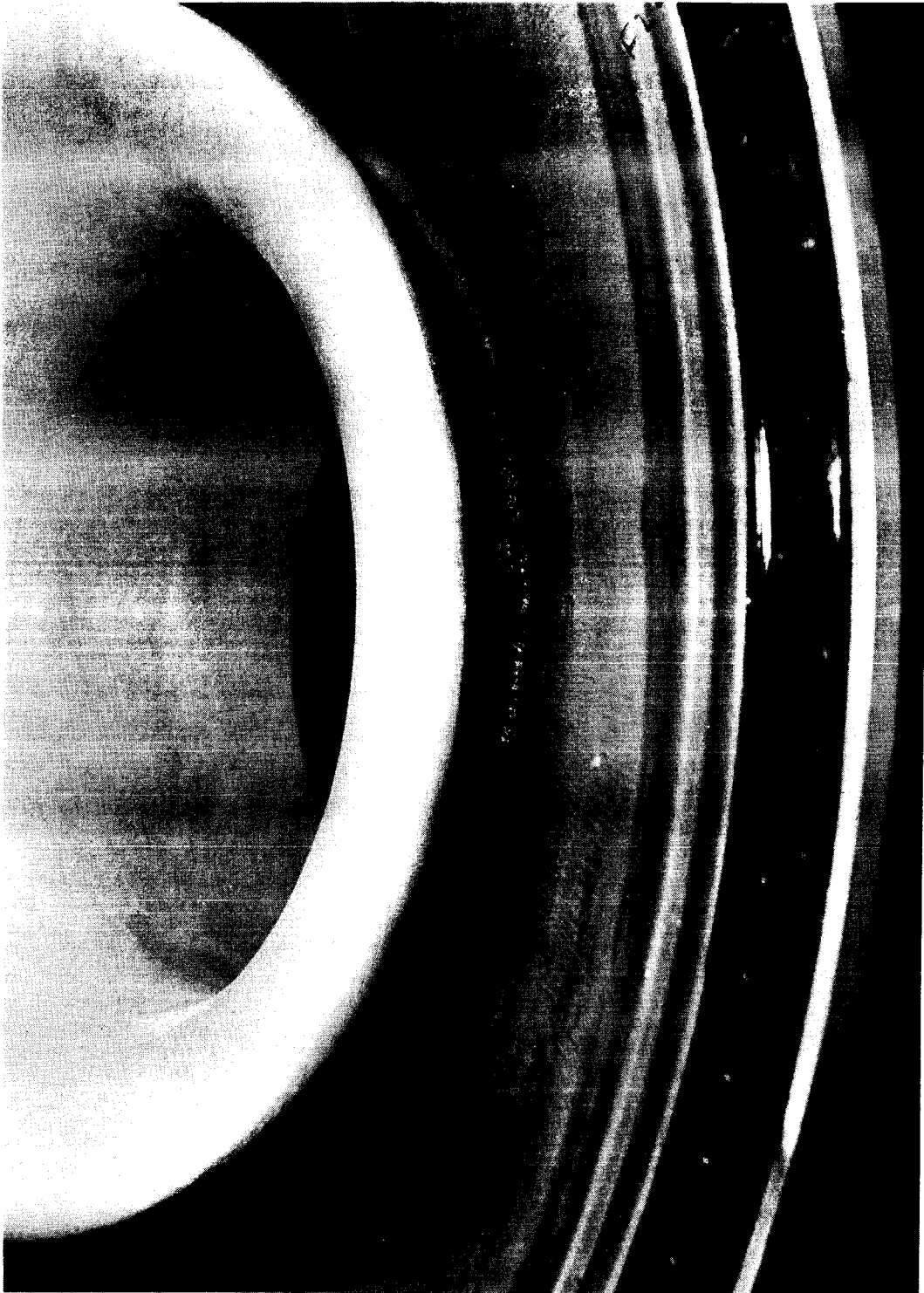
Nozzle Entrance Section During IBT-100 Application

Figure 22

Chamber Weight	483.9
Insulation	325.0
Liner (SD-850-2)	38.8
Propellant	7930.3
Restriction (IBT-106)	20.4
Nozzle	422.7
Igniter	23.9
Bolts, O-Rings, Miscellaneous	12.4
Potting Material (PR-1913)	7.2
V-61 Insulation	8.4
Total Assembly Weight	9273.0

Motor 44-SS-4 Weight Summary

Figure 23
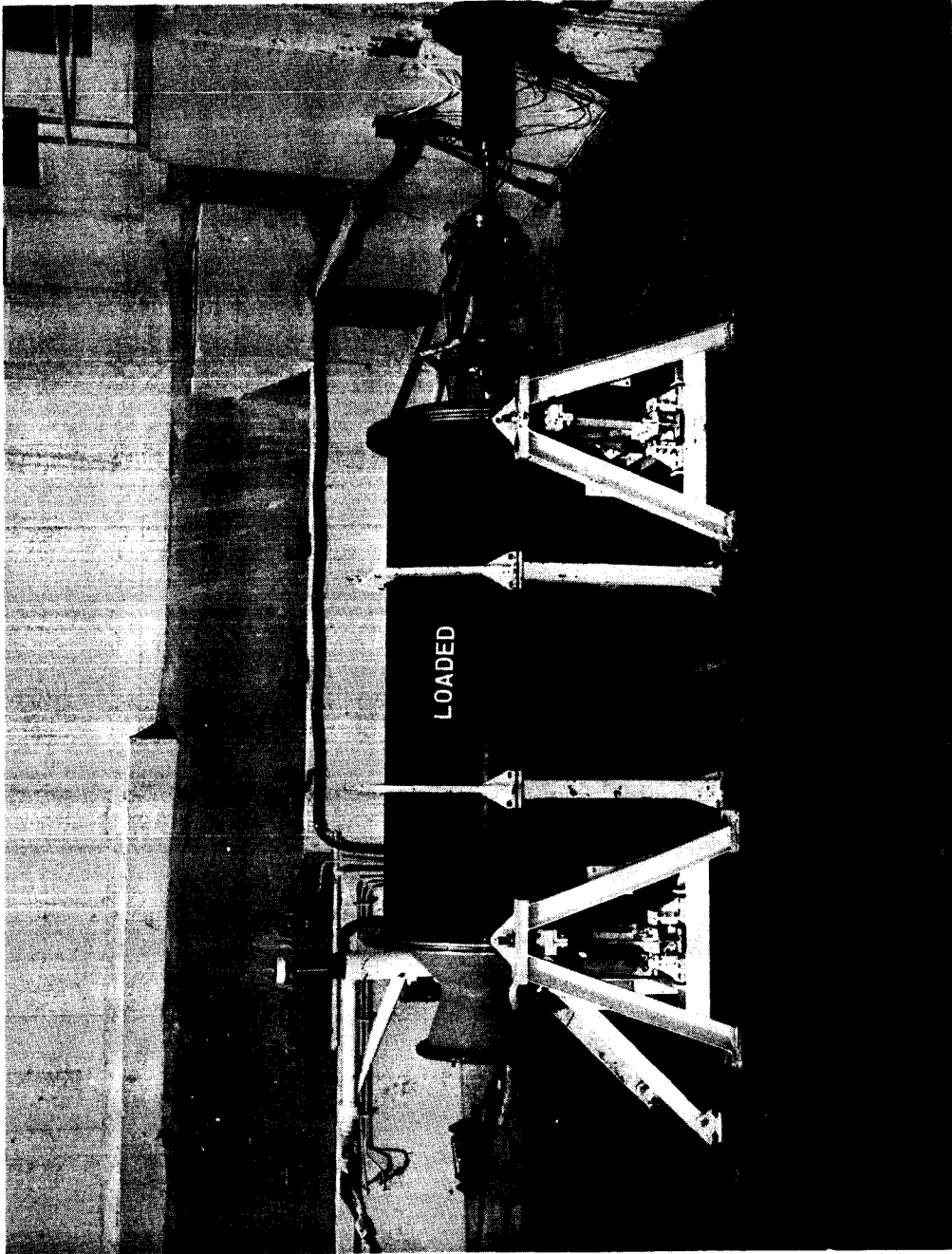
Motor 44-SS-4 in Test Fixture

Figure 24
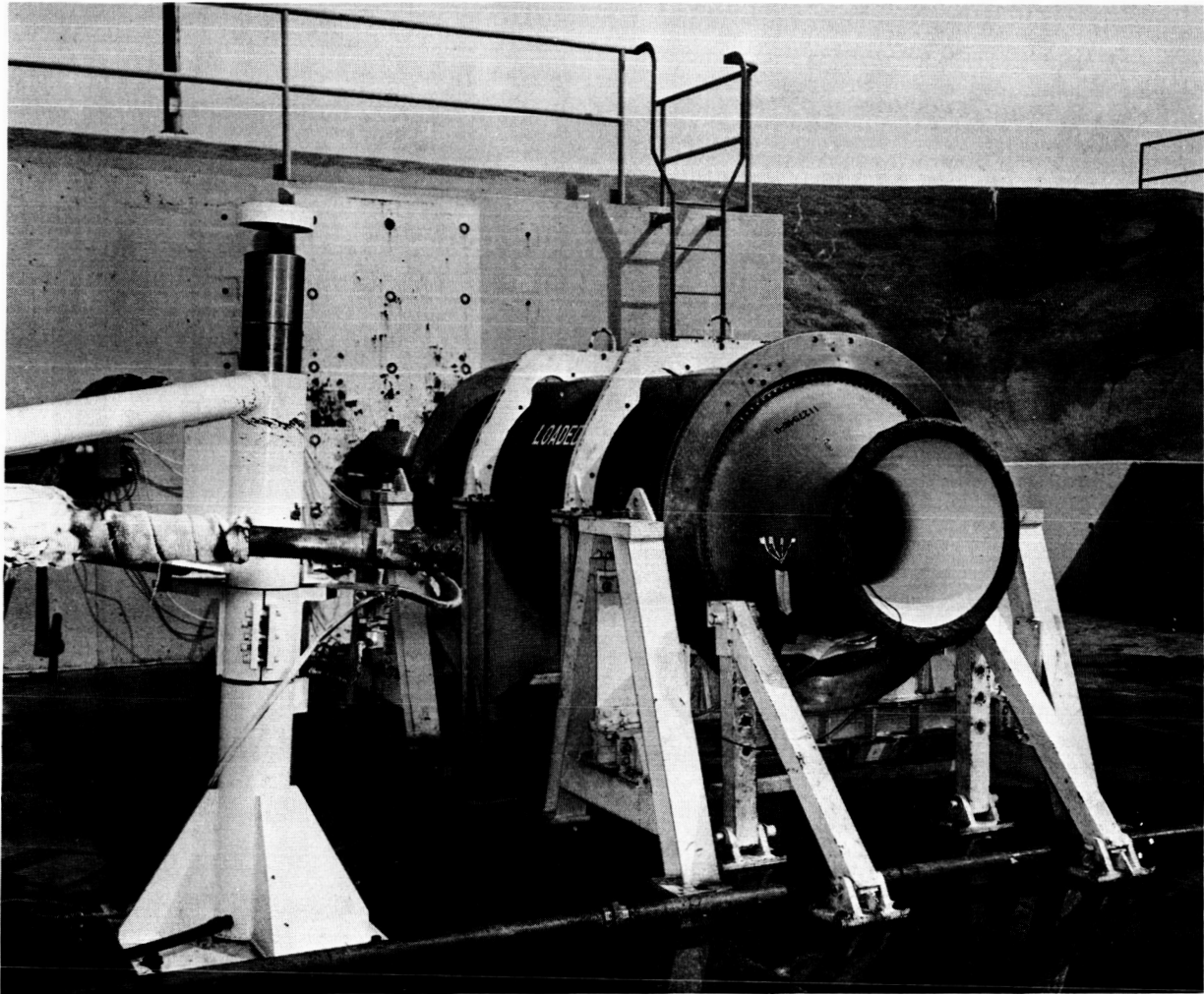
Prefire View of Motor 44-SS-4 Nozzle, 45° Aft

Figure 25

Prefire View of Motor 44-SS-4 Nozzle, 45° Aft

Figure 26
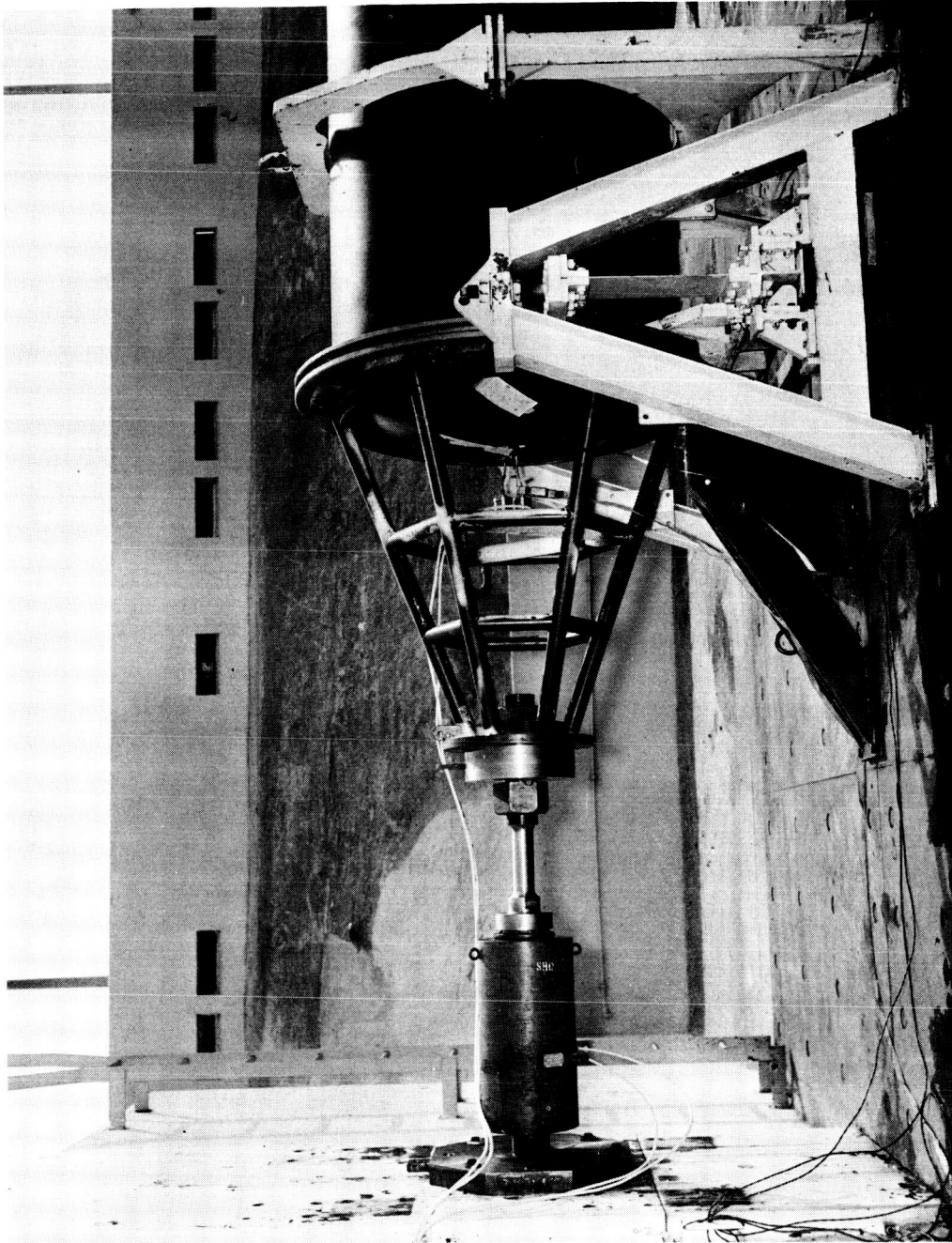
Test Set-Up, Thrust Measurement System and
Chamber Pressure Transducers

Figure 27
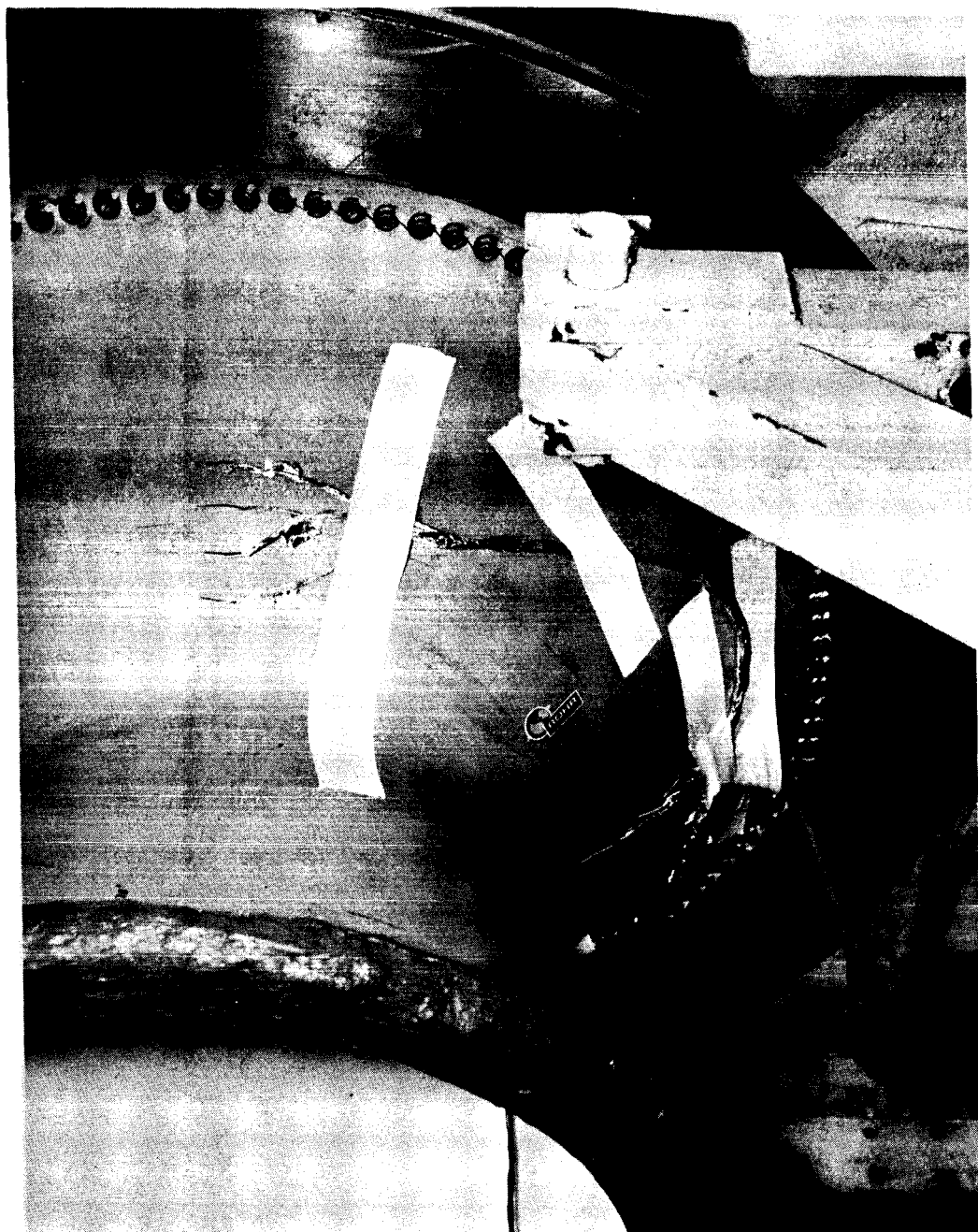
Typical Thermocouple Installation

Figure 28

T + 00.000 sec   Fire switch actuation

T + 00.052 sec   75% initial steady state pressure (igniter interval)

T + 04.271 sec   Maximum chamber pressure (606 psia)

T + 12.152 sec   End of web-action time

T + 13.382 sec   End of action time

T + 20.10   sec   Quench boom insertion initiated

T + 22.00   sec   Quench water on

T + 23.70   sec   Zero chamber pressure

Time-Event Summary
Motor 44-SS-4 Static Test

Figure 29
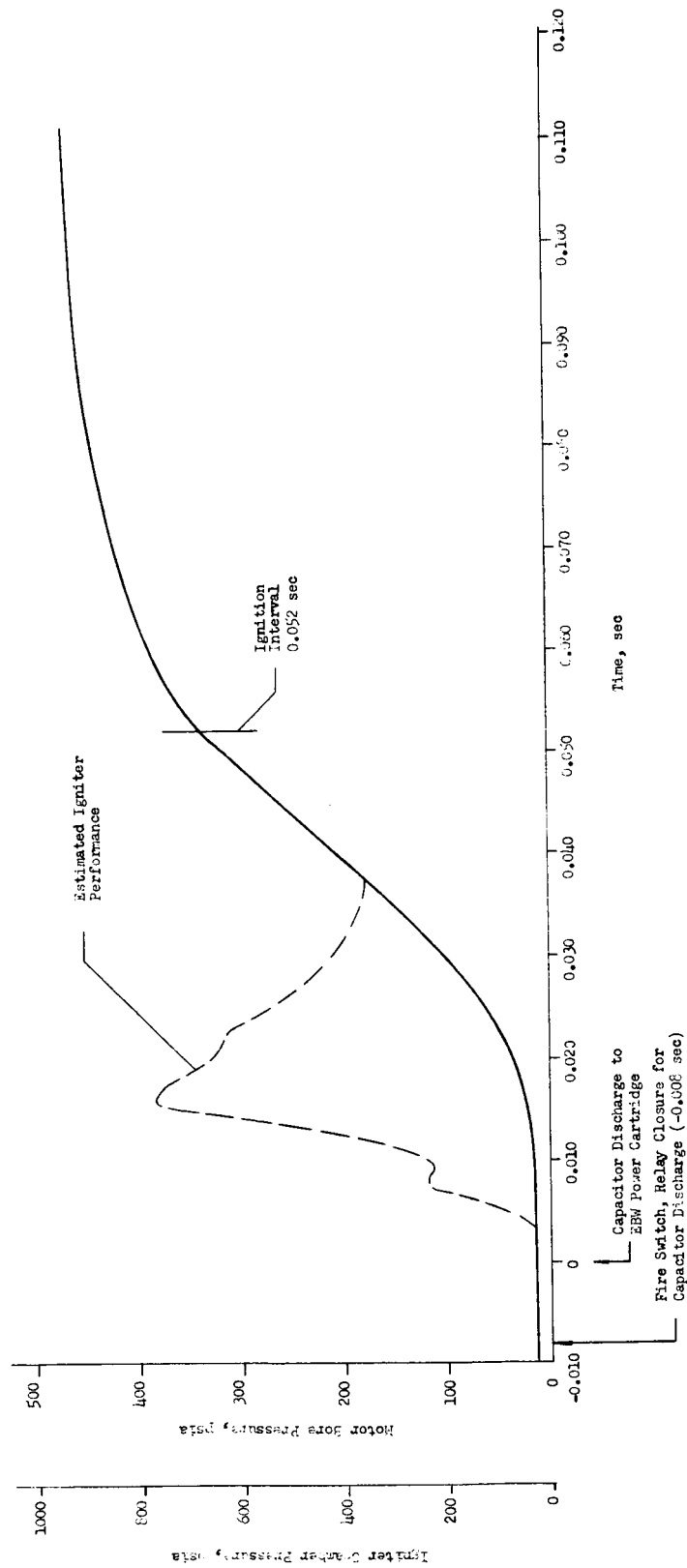
Ignition Transient, 44-SS-4 Static Test
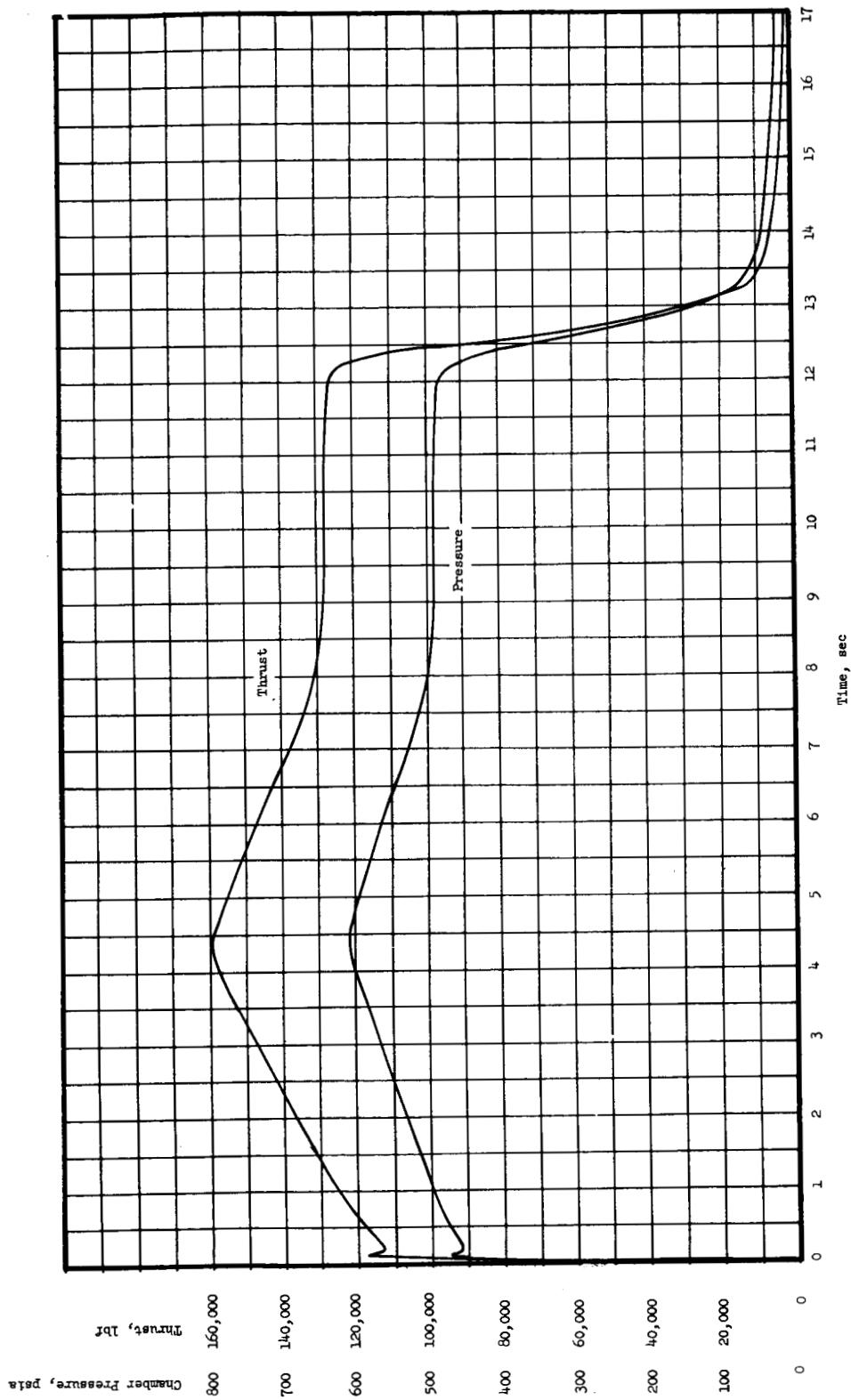
Figure 30

Pressure and Thrust vs Time Curves, Motor 44-SS-4

Figure 31

Total Impulse, lbf-sec	1,727,800
Standard Specific Impulse, lbf-sec/lbm	244.7
Delivered Specific Impulse, lbf-sec/lbm	217.9
Mass Flow Coefficient (C_W), lbm/lbf-sec	0.00629
Propellant Weight, lbm	7930
Web Action Time, sec	12.10
Action Time, sec	13.33
Maximum Chamber Pressure, psia	606
Average Chamber Pressure (Web Time), psia	522
Average Chamber Pressure (Action Time), psia	495
Maximum Thrust, lbf	157,870'
Average Thrust (Web Time), lbf	135,280
Average Thrust (Action Time), lbf	128,090

Motor 44-SS-4 Performance Summary

Figure 32
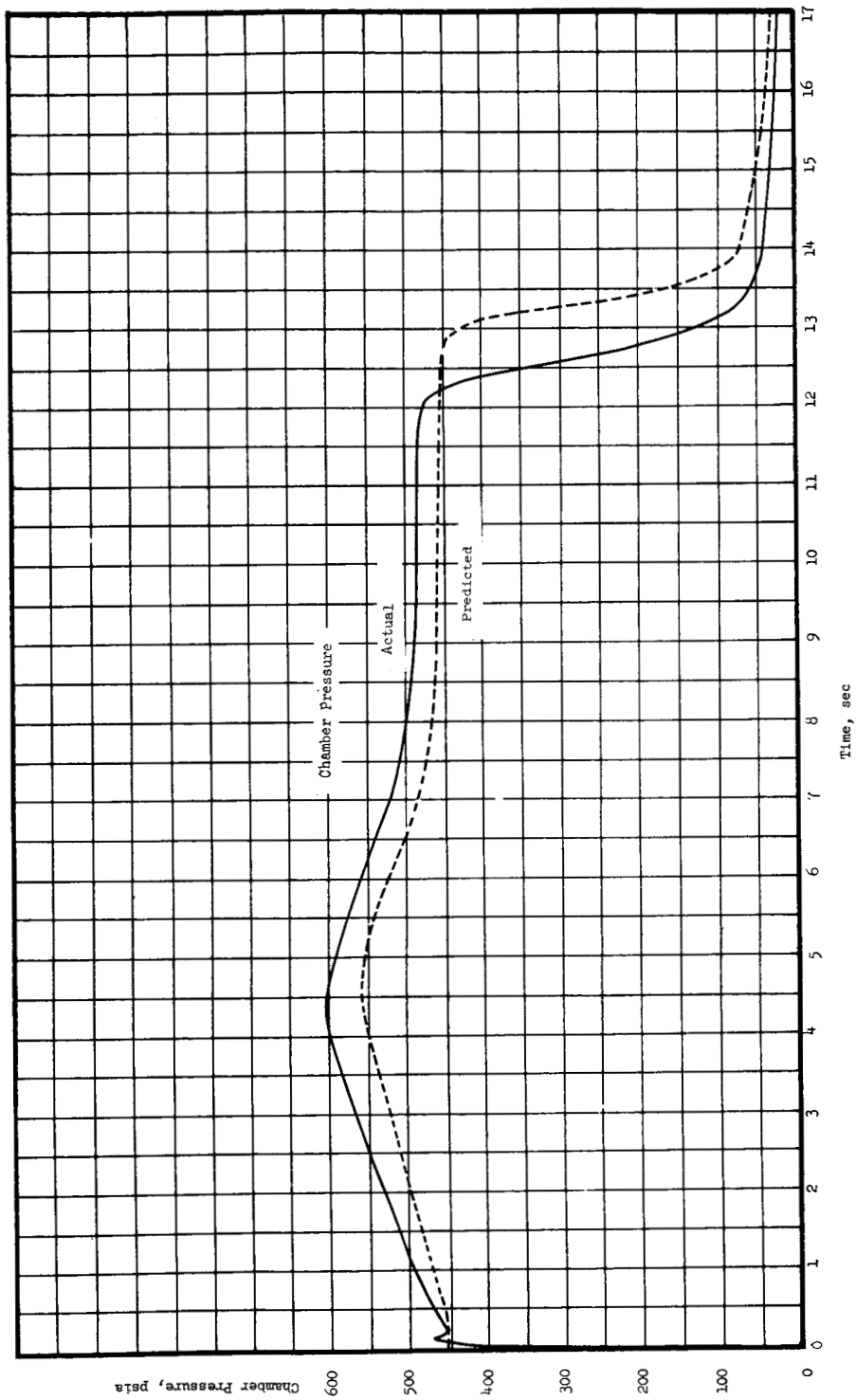
Predicted and Actual Pressure vs Time Curves, Motor 44-SS-4
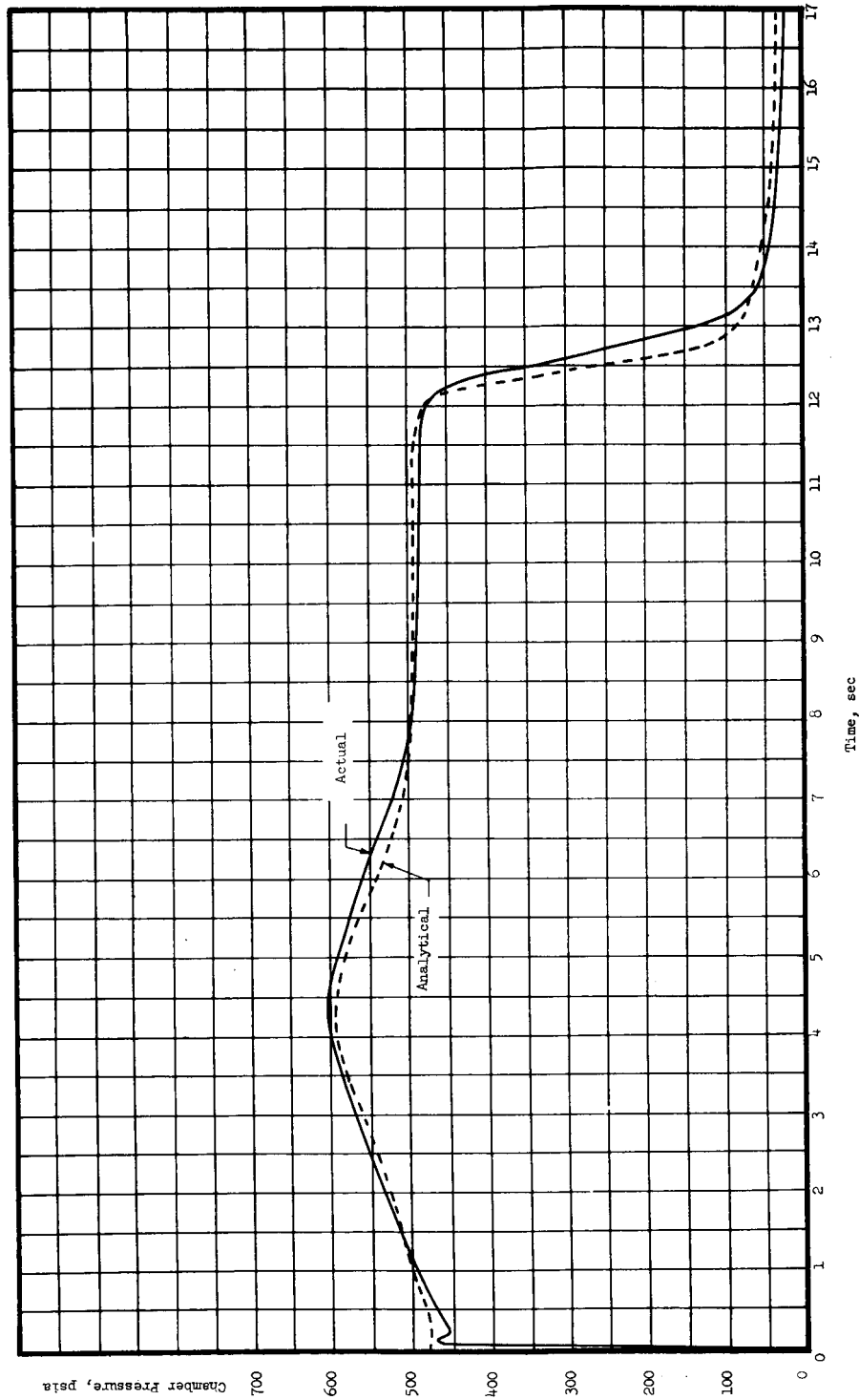
Figure 33

Analytical and Actual Pressure vs Time Curves, Motor 44-SS-4

Figure 34

Posttest View of Chamber Insulation

Figure 35
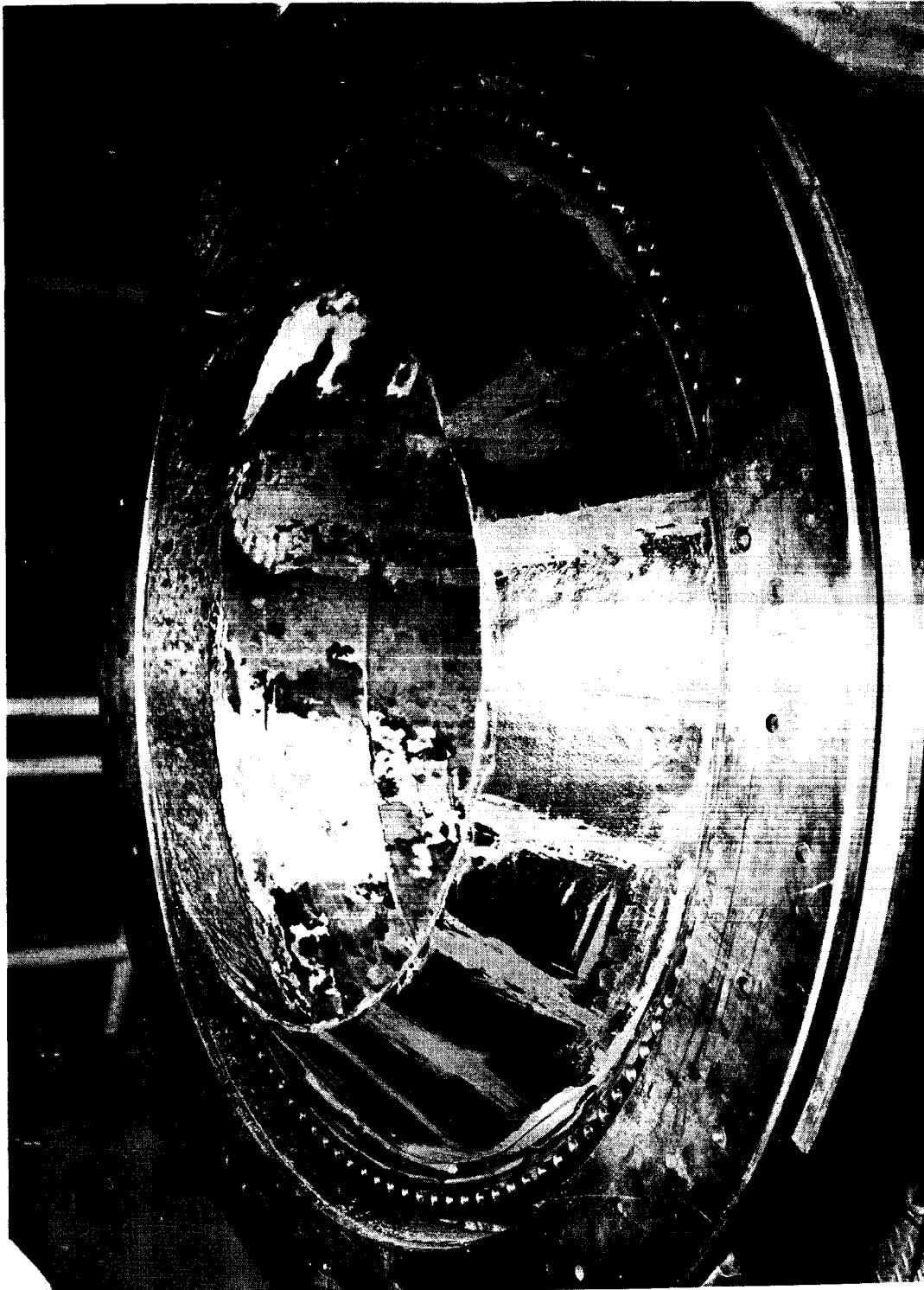
Posttest View of IBT-106 Grain Restrictor

Figure 36

Original
Thickness
(0.388 ± .012-in)

Char

Cross-Section
at 0° Location

Uncharred
IBT-106

| | 2.2 | | 1.8 | |
| C | | B | | A |
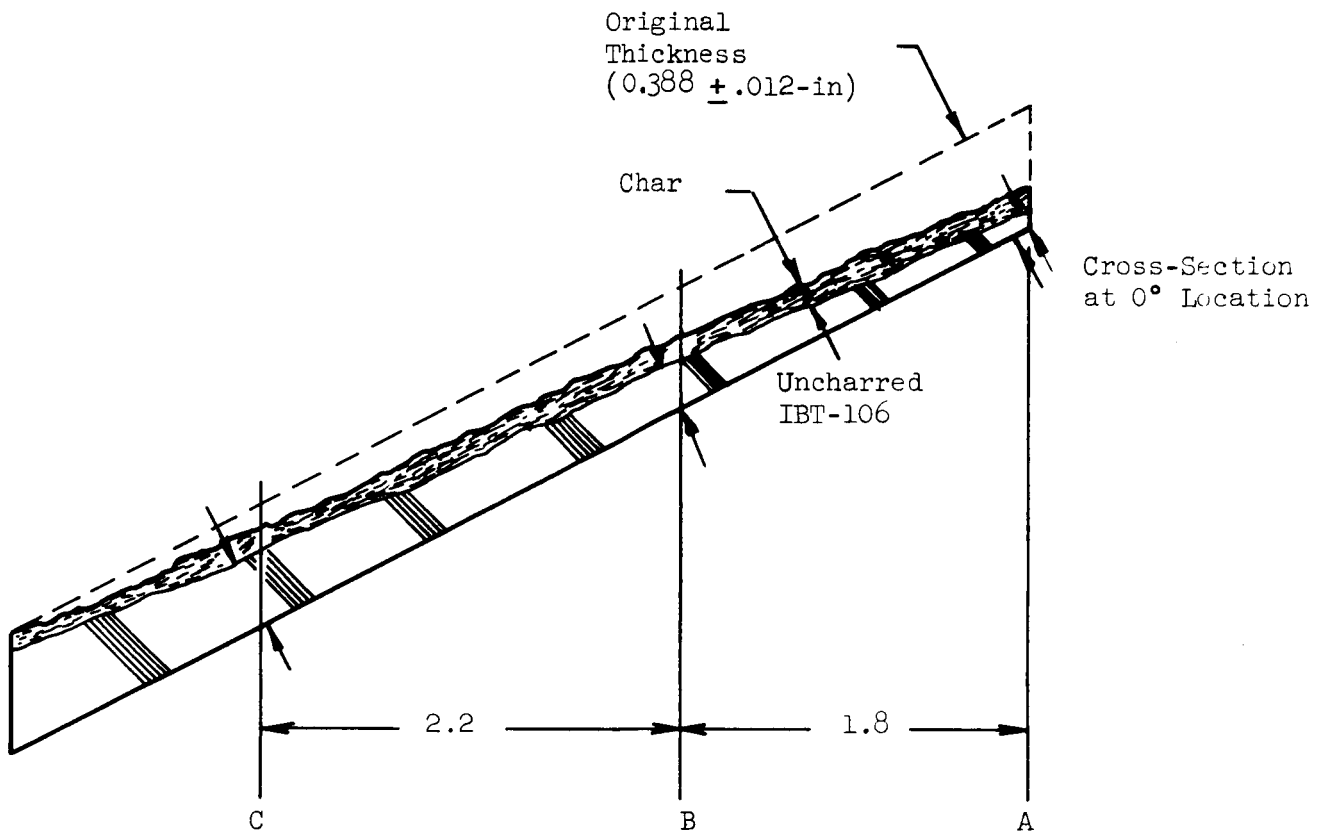
SECTION	EXPOSURE DURATION (secs)	MATERIAL LOSS (in)	LOSS RATE (in/sec)
A	12.1	.29	0.024
B	8.6	.17	0.020
C	4.3	.10	0.023

Performance of IBT-106 Restriction at Location of Maximum Erosion

Figure 37

Nozzle Shell Insulation Stations for Performance Summary
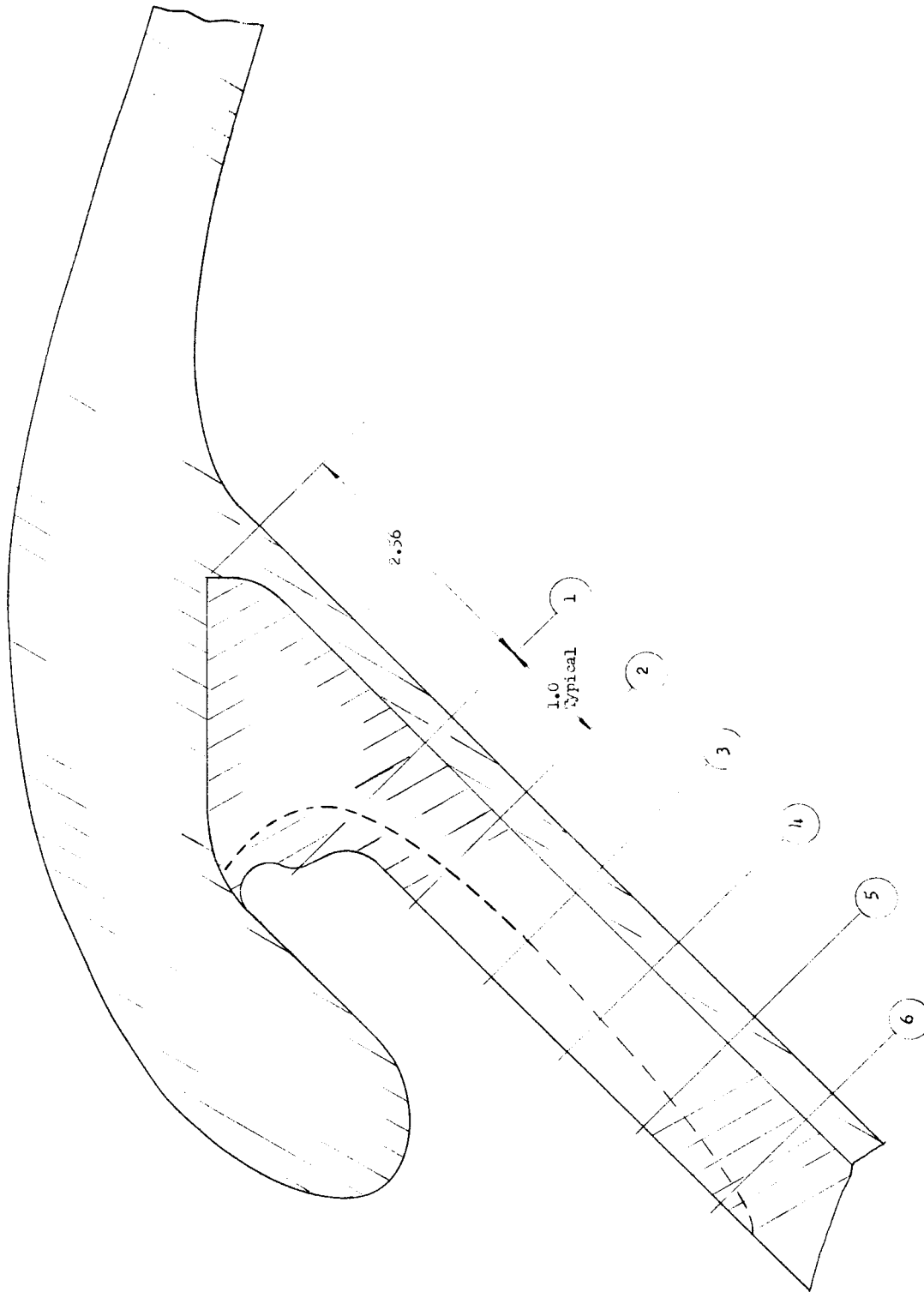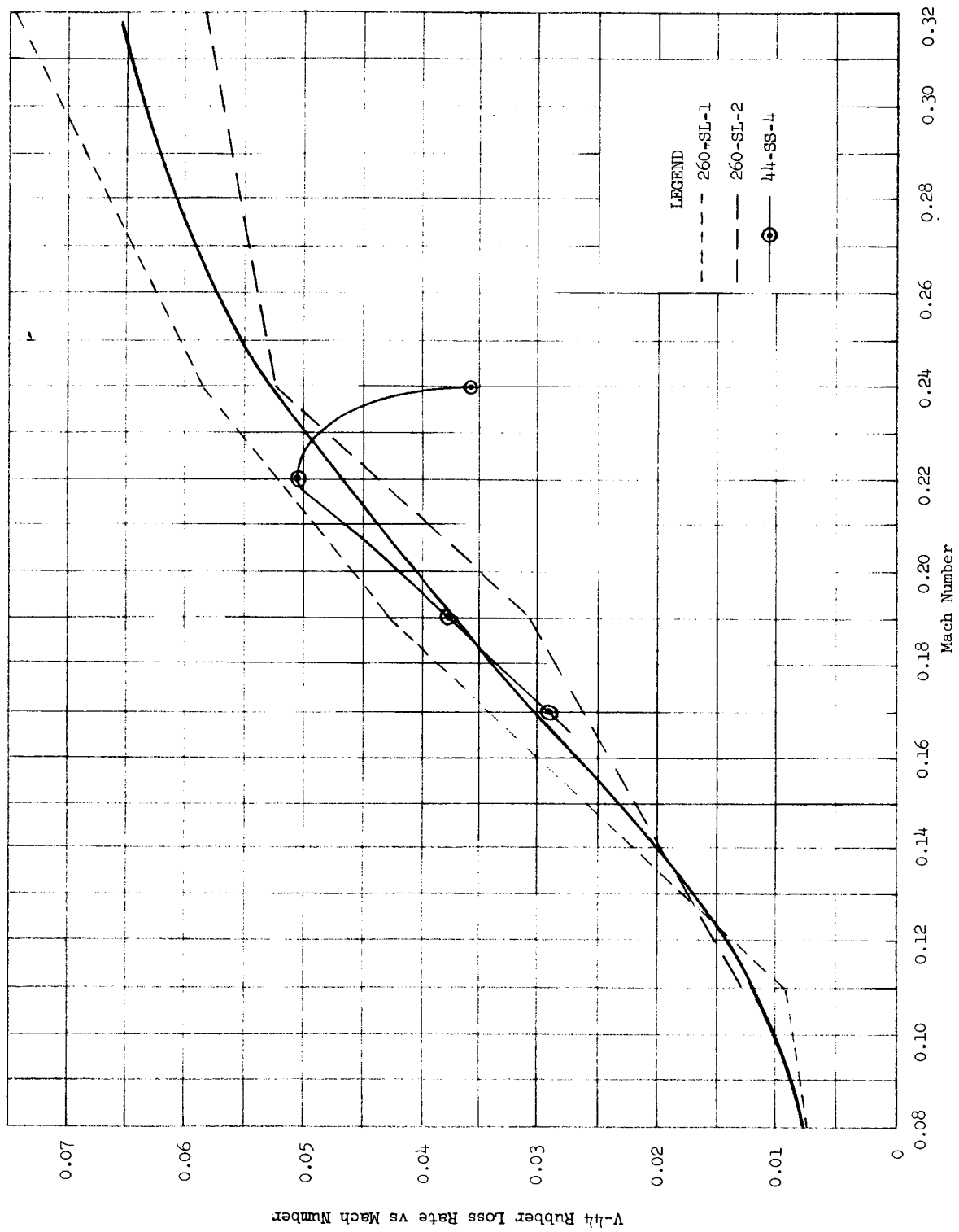
Figure 38

V-44 Rubber Loss Rate vs Mach Number

Figure 39
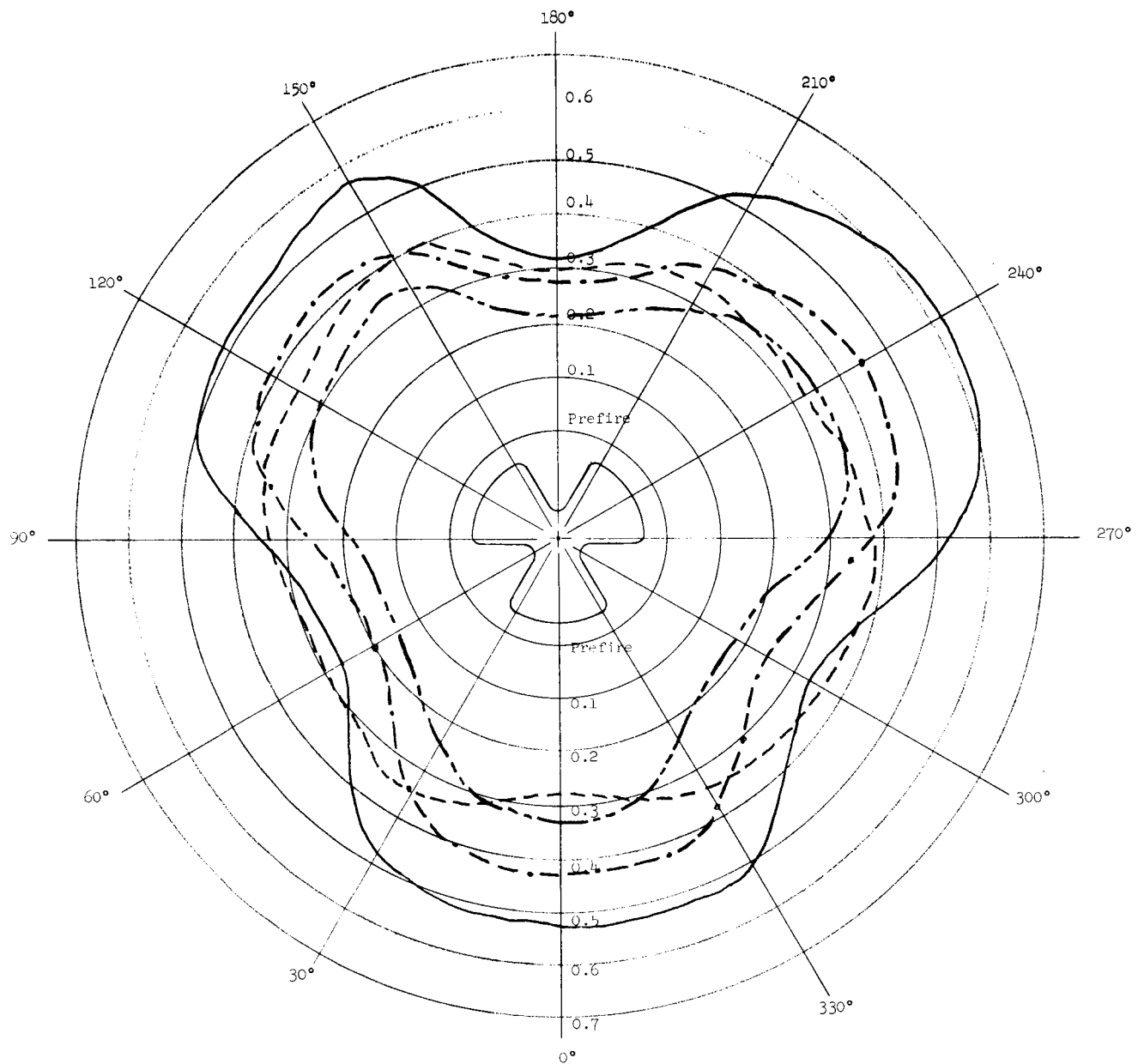
Nozzle Shell Insulation Erosion Pattern

Figure 40
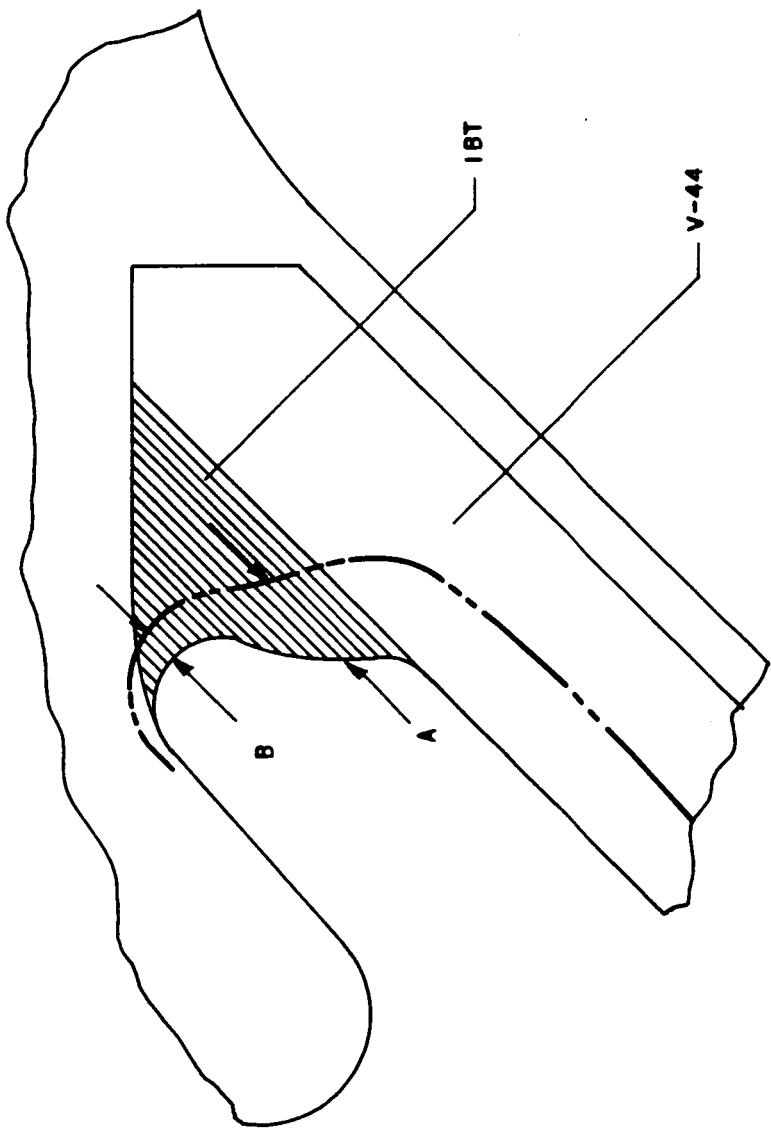
LOCATION, DEGREES

DIMENSION	0	60	120	180	240	300
A	0.31	0.23	0.31	0.26	0.33	0.21
B	0.01	0.18	0.06	0.05	0.02	0.08

IBT-100 Material Loss Summary

Figure 41, Sheet 1 of 2
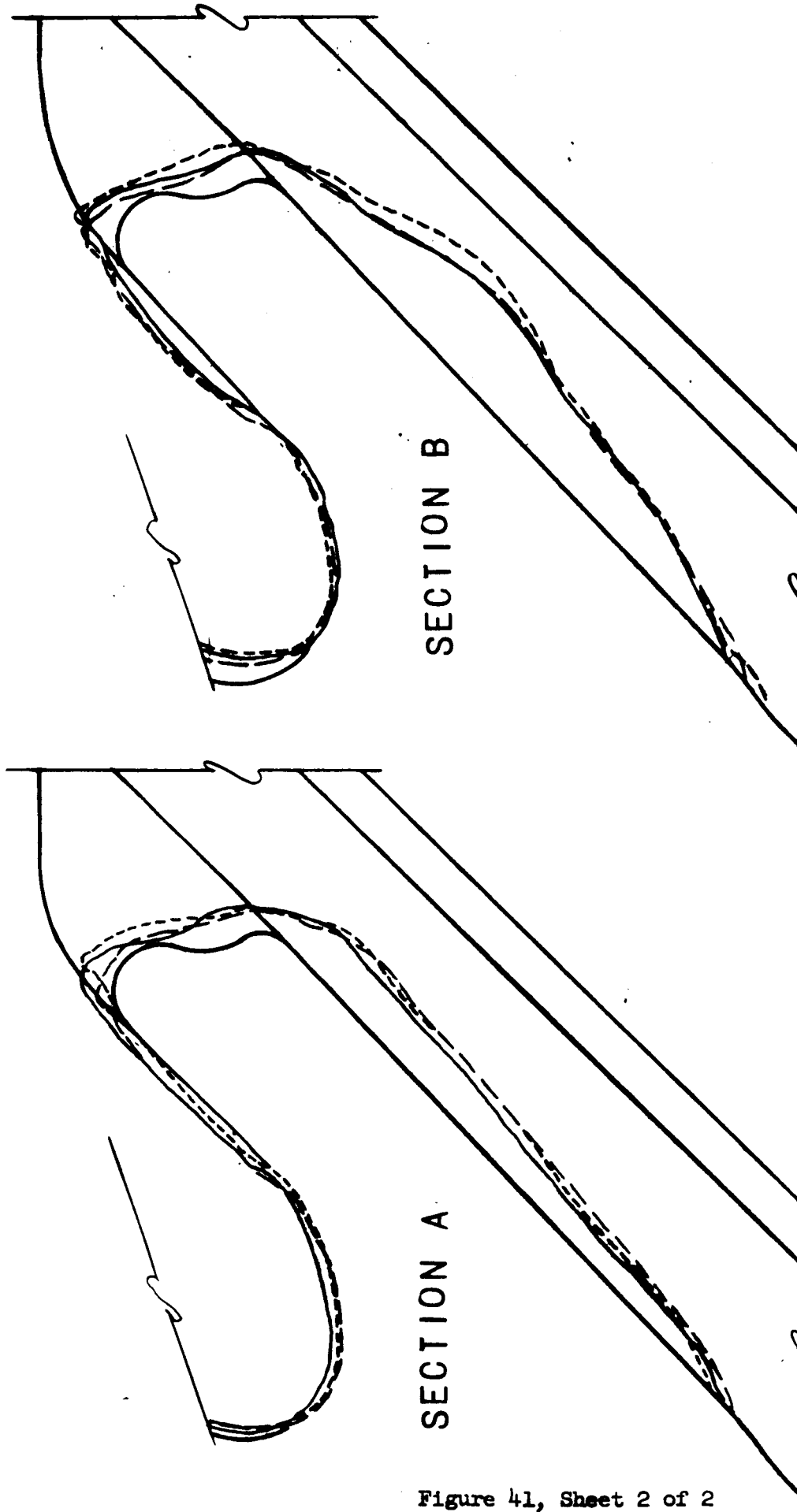
SECTION B

SECTION A

SYMBOL	DESCRIPTION		SECTIONS	
			A	B
	PRE-FIRE CONTOUR			
	HEAVY SOLID LINE		60° STA	0° STA
	LIGHT SOLID LINE		180° STA	120° STA
	LONG DASH LINE		300° STA	240° STA
	SHORT DASH LINE			

IBT-100 Material Loss Summary

Figure 41, Sheet 2 of 2

Area Ratio in 260-SL-3 Nozzle Shell	Equivalent Station in 44-SS-4 Nozzle Shell (Figure 38)	Material Thickness, in.			Maximum Expected Thickness(1) Loss, in.	Safety Factor	
		IBT-100	V-44	Total		(1)	(2)
2.8	3	4.50	5.30	9.80	3.92	1.35	2.5
3.2	4	3.45	5.30	8.75	3.5	1.57	2.5
3.5	5	1.70	5.40	7.10	2.2	2.46	3.2

(1) Assumes the following:

   a. IBT-100 thickness loss rate is the same as V-44 rubber at each area ratio.

   b. Exposure time at web average pressure is 75 sec.

   c. Exposure time at reduced pressure (tailoff and afterburn) is 20 sec.

(2) Excluding IBT-100 material thickness.

(3) Including IBT-100 material thickness.

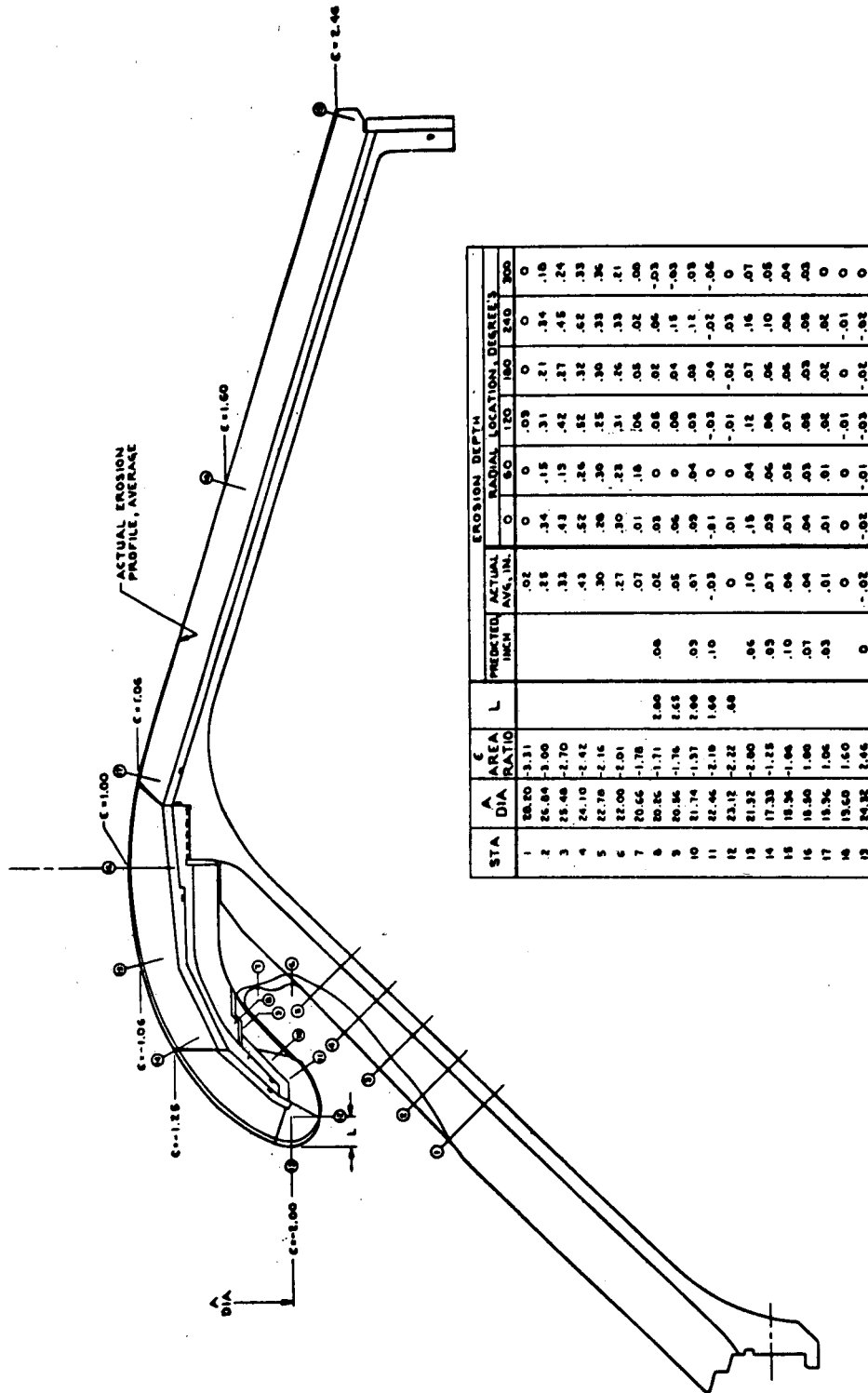Predicted Safety Factors for
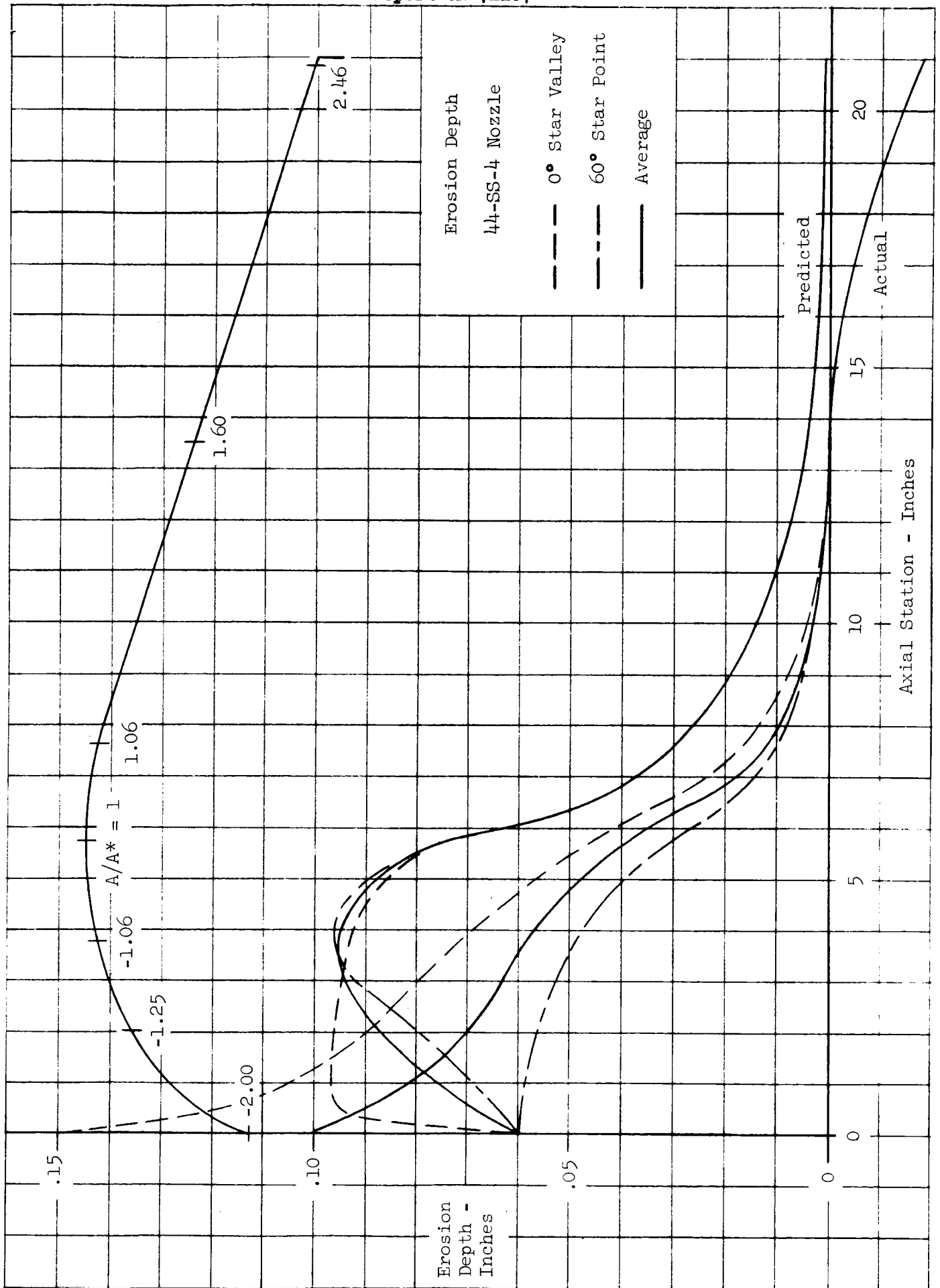260-SL-3 Motor Nozzle Shell Insulation

Figure 42

Nozzle Erosion Depths

Figure 43

Predicted and Actual Nozzle Erosion vs Area-Ratio

Figure 44

270°

SCALE
1 Inch R = 0.04

Grain Core
Profile

$\epsilon = 1.00$

$\epsilon = -1.06$

$\epsilon = -1.25$

$\epsilon = -2.00$

180°

0°

90°

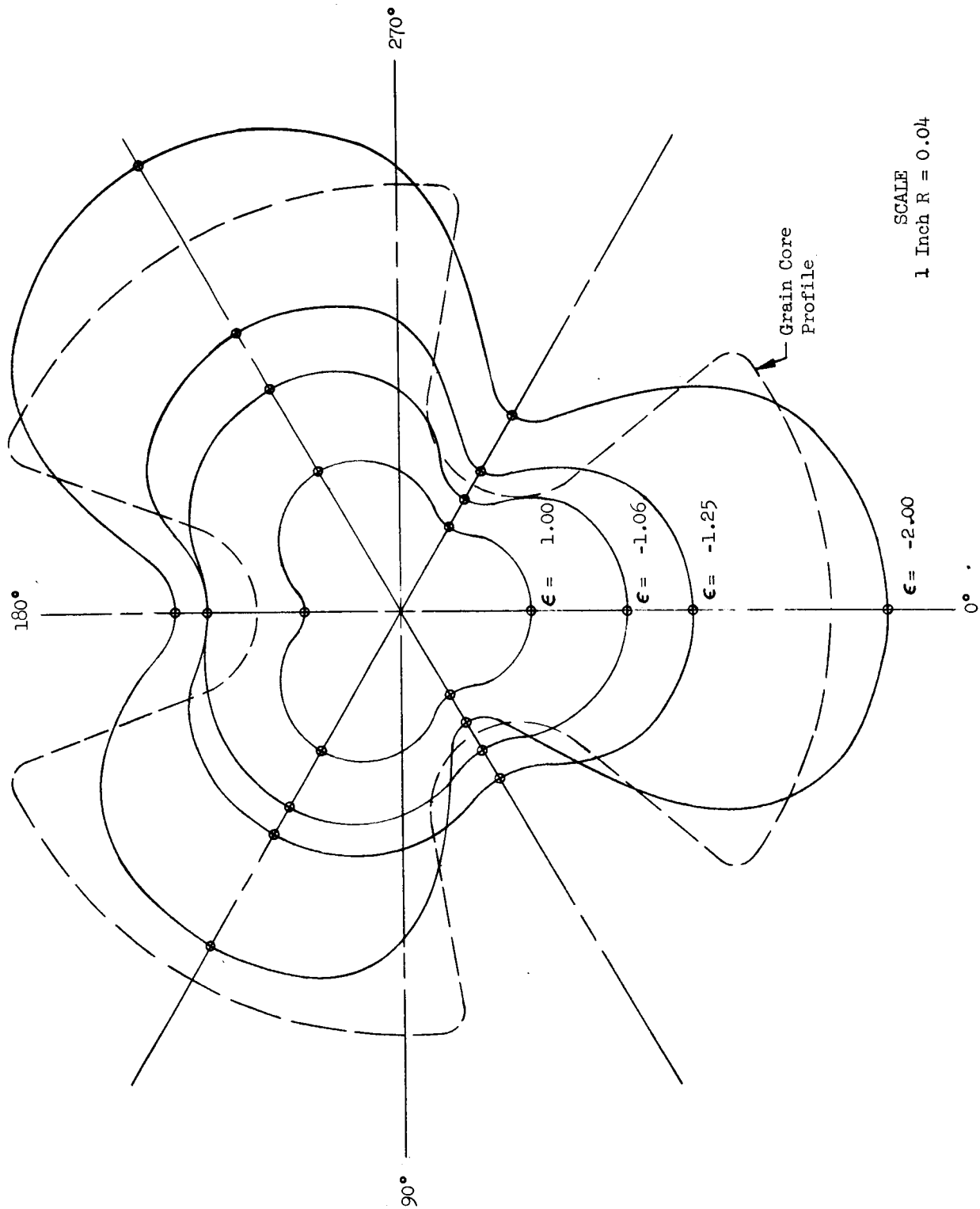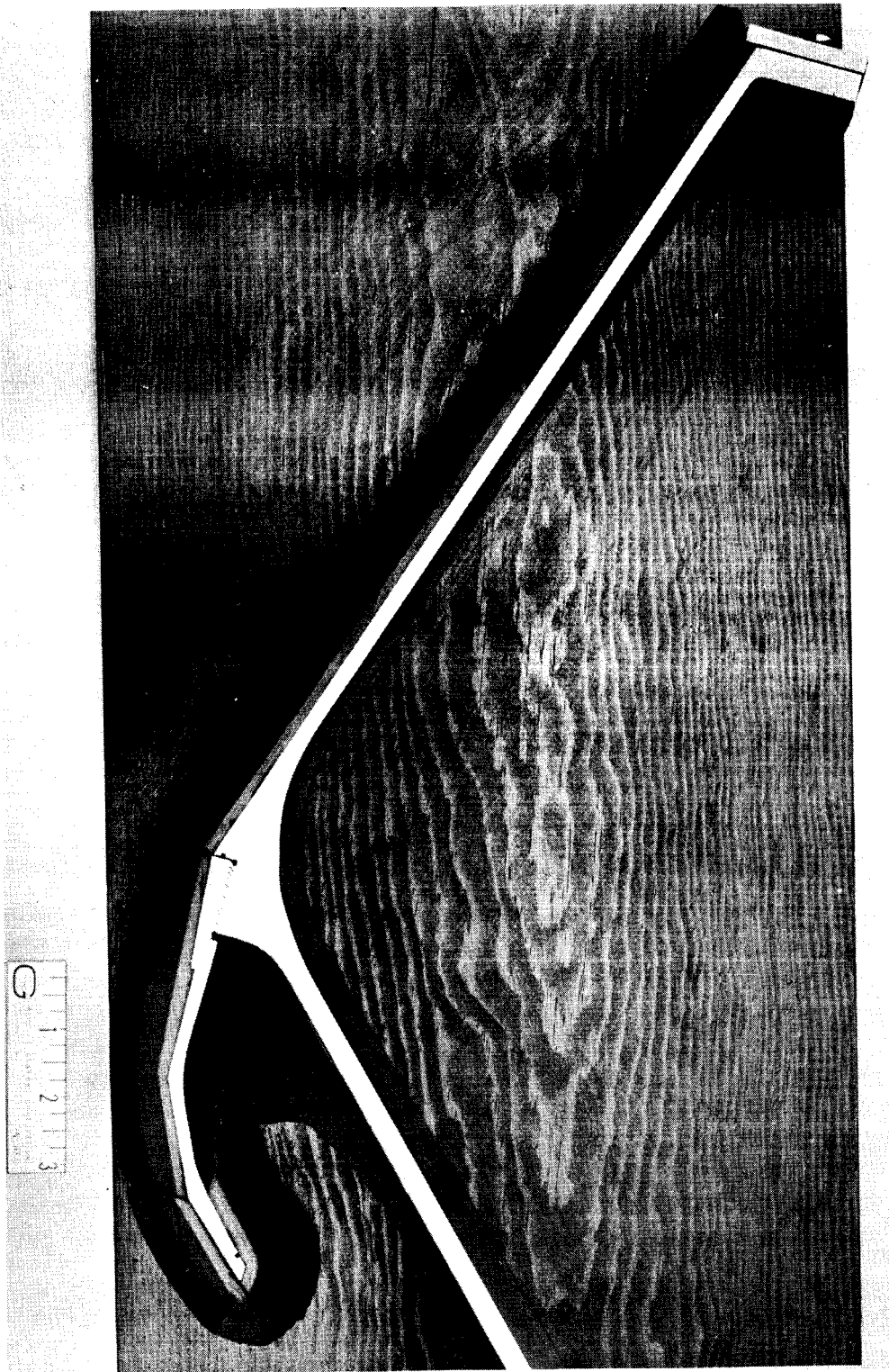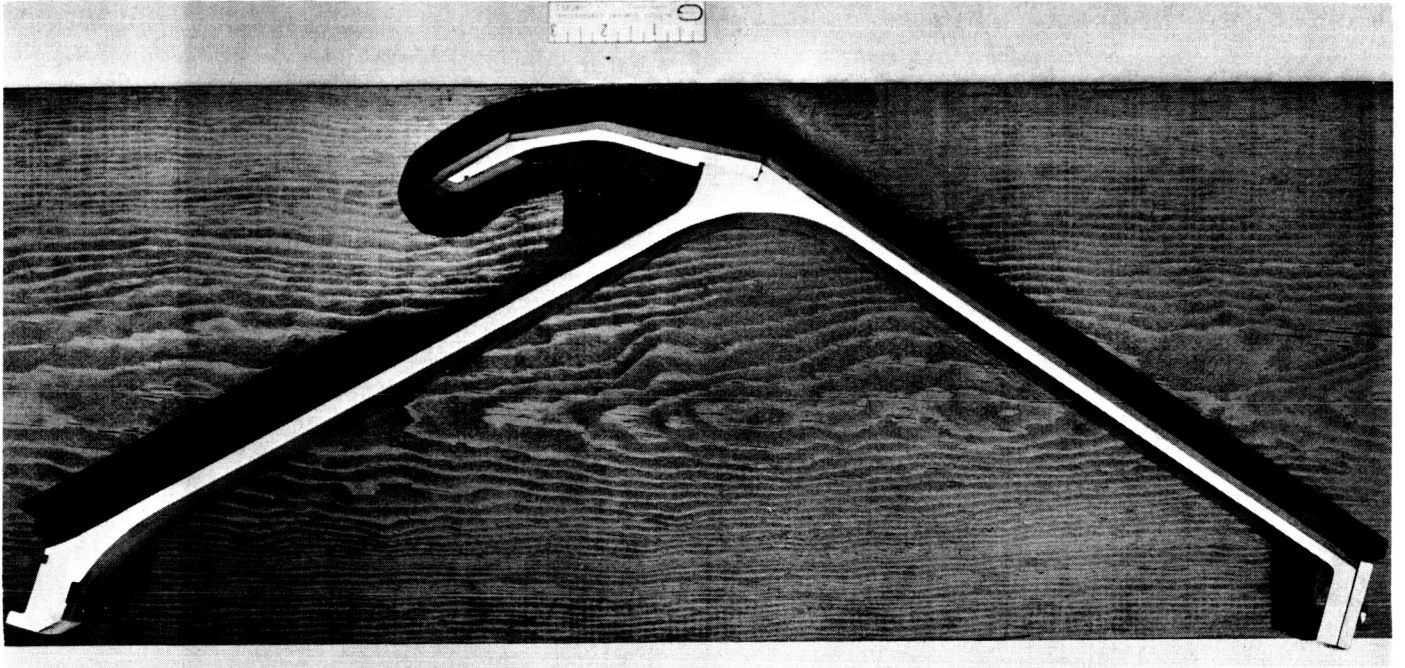Circumferential Erosion Comparison

Figure 45

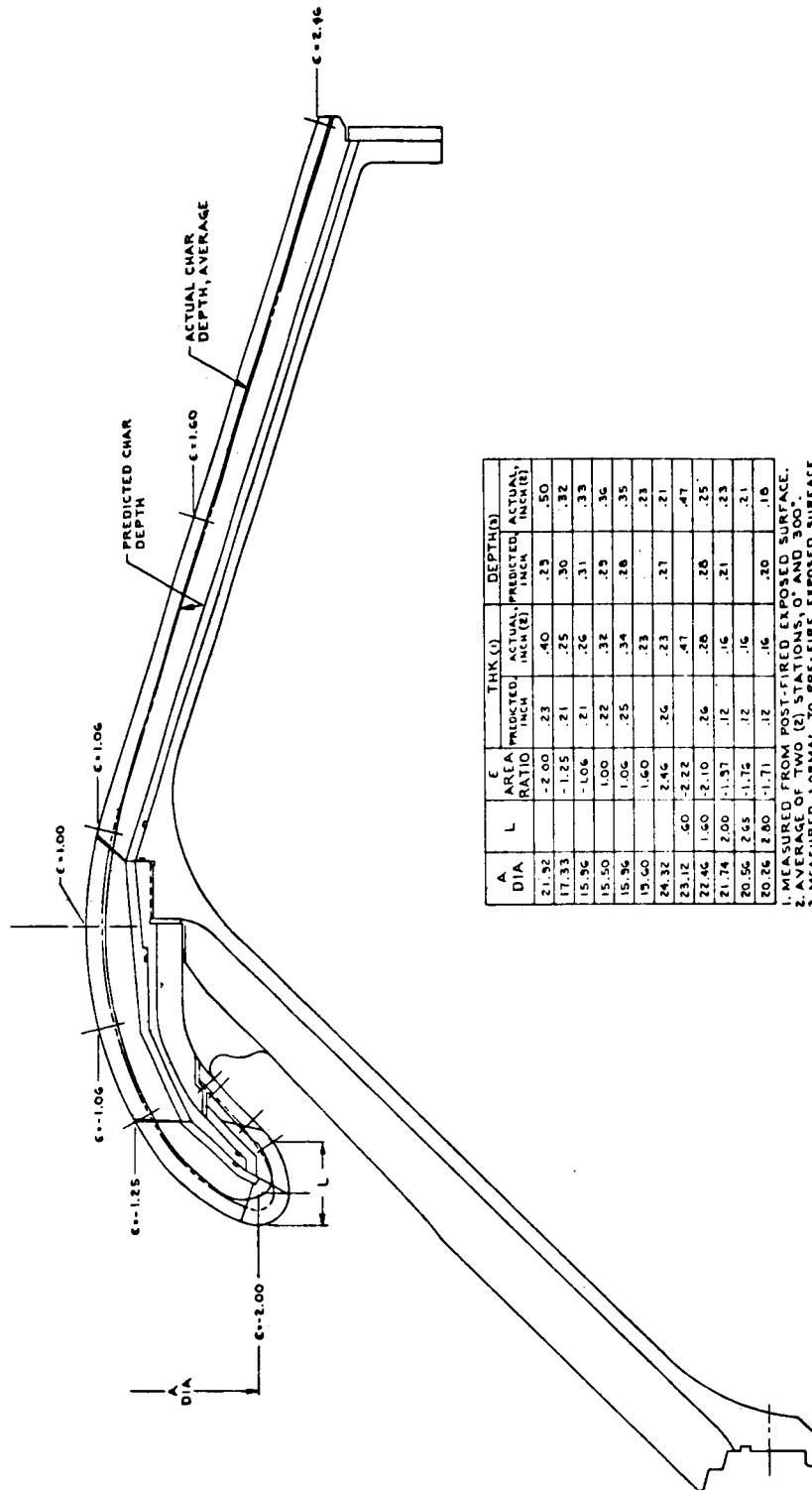Posttest View of 44-SS-4 Nozzle Cross-Section

Figure 46

Cross-Section of 44-SS-4 Nozzle at 0° Orientation

Figure 47

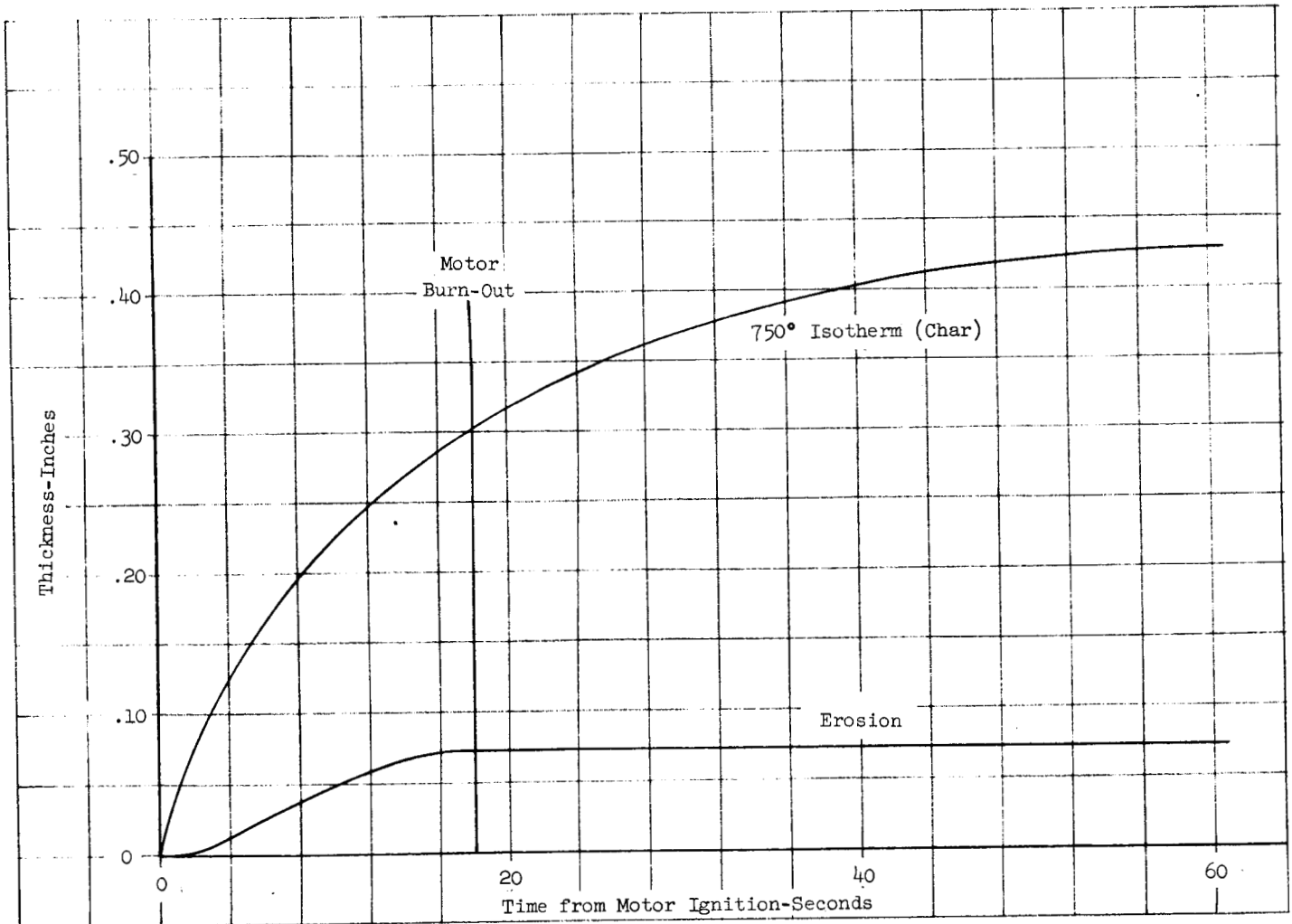0° Section of 44-SS-4 Nozzle, Posttest View

Figure 48

A DIA	L	ε AREA RATIO	THK (1) PREDICTED INCH	ACTUAL INCH (2)	DEPTH(3) PREDICTED INCH	ACTUAL INCH (3)
21.52		-2.00	.23	.40	.23	.50
17.33		-1.25	.21	.25	.30	.32
15.96		-1.06	.21	.26	.31	.33
15.50		1.00	.22	.32	.29	.36
15.96		1.06	.25	.34	.28	.35
15.60		1.60	.26	.23		.23
24.32		2.46		.23	.21	.21
23.12	.60	-2.22				.47
22.46	1.60	-2.10	.26	.28	.28	.25
21.74	2.00	-1.57	.12	.16	.21	.23
20.56	2.65	-1.75	.12	.16		.21
20.26	2.80	-1.71	.20	.16	.20	.18

1. MEASURED FROM POST-FIRED EXPOSED SURFACE.
2. AVERAGE OF TWO (2) STATIONS, 0° AND 300°.
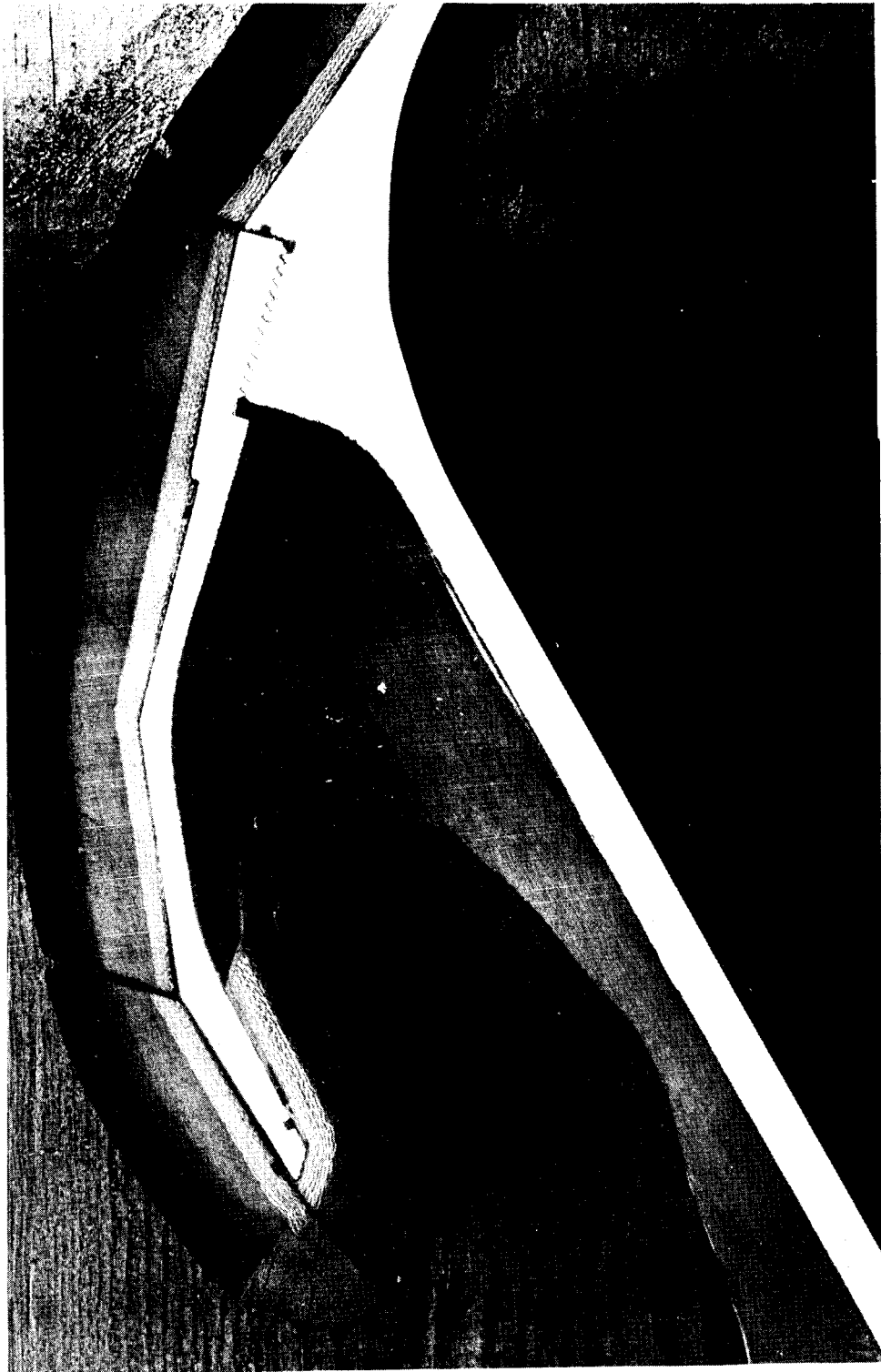3. MEASURED NORMAL TO PRE-FIRE EXPOSED SURFACE.

Nozzle Char Depths

Figure 49

Predicted Erosion and Char Depths at 44-SS-4 Throat Station

Figure 50

Enlarged View of 0° Cross-Section of 44-SS-4 Nozzle

Figure 51